Mechanics and Materials Center
TEXAS A&M UNIVERSITY
College Station, Texas

EXPERIMENTAL AND THEORETICAL DETERMINATION OF THE
THERMOMECHANICAL RESPONSE OF INELASTIC STRUCTURAL
MATERIALS TO HIGH ENERGY THERMAL INPUTS

Semi-Annual Technical Report

Submitted by

D.H. Allen
Aerospace Engineering Department

and

M.S. Pilant
Mathematics Department

Texas A&M University
College Station, Texas 77843

to the

Air Force Office of Scientific Research
Office of Aerospace Research
United States Air Force

DTIC
ELECTED
FEB 16 1989

AD-A206 100

REPORT DOCUMENTATION PAGE

Form Approved
OMB No. 0704-0186

1a. REPORT SECURITY CLASSIFICATION unclassified	1b. RESTRICTIVE MARKINGS

2a. SECURITY CLASSIFICATION AUTHORITY	3. DISTRIBUTION/AVAILABILITY OF REPORT
2b. DECLASSIFICATION/DOWNGRADING SCHEDULE	**Approved for public release, distribution unlimited**

4. PERFORMING ORGANIZATION REPORT NUMBER(S) MM 5485-88-10	5. MONITORING ORGANIZATION REPORT NUMBER(S) **AFOSR·TR· 89-0140**

6a. NAME OF PERFORMING ORGANIZATION Aerospace Engineering Dept.	6b. OFFICE SYMBOL (If applicable)	7a. NAME OF MONITORING ORGANIZATION Air Force Office of Scientific Research

6c. ADDRESS (City, State, and ZIP Code) Texas A&M University College Station, Texas 77843	7b. ADDRESS (City, State, and ZIP Code) Bolling AFB Washington, DC 20332

8a. NAME OF FUNDING/SPONSORING ORGANIZATION Air Force Office of Scientific	8b. OFFICE SYMBOL (If applicable) NA	9. PROCUREMENT INSTRUMENT IDENTIFICATION NUMBER F49620-86-K-0016

8c. ADDRESS (City, State, and ZIP Code) Bolling AFB Washington, DC 20332	10. SOURCE OF FUNDING NUMBERS			
	PROGRAM ELEMENT NO. 61102F	PROJECT NO. 2302	TASK NO. B1	WORK UNIT ACCESSION NO.

11. TITLE (Include Security Classification)

Experimental and Theoretical Determination of the Thermomechanical Response of Inelastic Structural Materials to High Energy Thermal Inputs – Semi-Annual Report (u)

12. PERSONAL AUTHOR(S)
D.H. Allen and M.S. Pilant

13a. TYPE OF REPORT semi-annual	13b. TIME COVERED FROM July '88 TO Dec '88	14. DATE OF REPORT (Year, Month, Day) December 1988	15. PAGE COUNT

16. SUPPLEMENTARY NOTATION

17. COSATI CODES			18. SUBJECT TERMS (Continue on reverse if necessary and identify by block number)
FIELD	GROUP	SUB-GROUP	laser heating, constitutive properties) viscoplasticity; heat transfer \ finite element methods, thermomechanics .

19. ABSTRACT (Continue on reverse if necessary and identify by block number)

The general objective of this research is to improve on existing theoretical models for predicting the response of inelastic aerospace structural components subjected to hostile thermal environments with emphasis on transient temperature conditions, radiation boundary conditions, extremely rapid heating rates, and possible phase change of the materials involved. For materials subjected to the conditions under study herein it is necessary to perform extremely complex experiments in order to determine the precise form of the theoretical constitutive equations. Finally, it is necessary to implement the resulting equations to boundary value problem solving algorithms in order to model the response of structural components with stress, strain, and temperature gradient fields.

20. DISTRIBUTION/AVAILABILITY OF ABSTRACT ☐ UNCLASSIFIED/UNLIMITED ☑ SAME AS RPT. ☑ DTIC USERS	21. ABSTRACT SECURITY CLASSIFICATION unclassified
22a. NAME OF RESPONSIBLE INDIVIDUAL A.K. Amos	22b. TELEPHONE (Include Area Code) (202) 767-4937 22c. OFFICE SYMBOL AFOSR/NA

DD Form 1473, JUN 86   Previous editions are obsolete   SECURITY CLASSIFICATION OF THIS PAGE
unclassified

EXPERIMENTAL AND THEORETICAL DETERMINATION OF THE
THERMOMECHANICAL RESPONSE OF INELASTIC STRUCTURAL
MATERIALS TO HIGH ENERGY THERMAL INPUTS

Semi-Annual Technical Report

Submitted by

D.H. Allen
Aerospace Engineering Department

and

M.S. Pilant
Mathematics Department

Texas A&M University
College Station, Texas 77843

to the

Air Force Office of Scientific Research
Office of Aerospace Research
United States Air Force

TABLE OF CONTENTS

INTRODUCTION

1.1 Summary

This report details results of research performed during the period June 1, 1988 through December 31, 1988 under AFOSR contract no. F49620-86-K-0016. The project was initiated in June 1986 and covers a duration of forty months.

The general objective of this research is to improve on existing theoretical models for predicting the response of inelastic aerospace structural components subjected to hostile thermal environments with emphasis on transient temperature conditions, radiation boundary conditions, extremely rapid heating rates, and possible phase change of the materials involved.

1.2 Statement of Work

Experimental and theoretical research are being performed to characterize the response of structural components subjected to transient temperature conditions resulting in inelastic material behavior. The research is being performed in the following stages:

1) theoretical development of thermodynamic constraints on inelastic materials under transient temperature conditions;

2) development of modified heat conduction equations to account for two-way thermomechanical coupling in these inelastic materials;

3) experimentation to determine further constraints on inelastic materials under transient temperature conditions;

4) development of multi-dimensional theoretical algorithms for predicting response of the inelastic structural components described above; and

5) experimentation to verify the theoretical algorithms described in item 4).

Items 1) through 4) above are being performed entirely on the main campus at Texas A&M University. Item 5) will be performed both at the Air Force Wright Aeronautics Laboratory at Wright Patterson Air Force Base and Texas A&M University. Details of this interaction will be described further below.

RESEARCH COMPLETED

2.1 Summary of Completed Research

Research during the period June 1 through December 31, 1988 is summarized below:

1) additional computational results have been obtained utilizing the one-way coupled model discussed in reference 1;

2) two new two-way coupled models are under development at this time;

3) the initial plate experiments have been performed at AFWAL and the second set of plate experiments is being prepared at this time;

4) the constitutive tests on Hastelloy X are underway; and

2

5) computational facilities have been upgraded to perform the theoretical analyses.

2.2 Expected Research

The following results are expected between now and Sept. 30, 1989:

1) the plate experiments will be completed at AFWAL;

2) the one-way coupled model will be compared to the plate experiments;

3) the two-way coupled model will be completed and compared to the plate experiments; and

4) the constitutive tests on Hastelloy will be completed.

2.3 Theoretical Developments

A brief description of theoretical progress over the past six months is given below.

2.3.1 One-Way Coupled Model

The one-way coupled model has been completed and documented in reference 1 (See Appendix 6.1). Recently this model has been used to predict the response of a circular plate subjected to the instantaneous heat pulse shown in Fig. 1. As shown in Fig. 2, the model predicts a dynamic response which is not unlike resonance. Figure 3 shows the displacement profile during a single cycle of response, demonstrating that a permanent out-of-plane

3

deformation caused by the thermal field constrains this dynamic response. Figures 4 through 7 show that significant stresses occur which causes substantial inelastic strain near the center of the plate.

In our next series of experiments we will be attempting to determine the veracity of this dynamic response as predicted by the model.

2.3.2 Two-way Coupled Models

We are currently placing the emphasis in model development on the construction of two-way coupled algorithms for analyzing the plate problem.

The two-way coupled problem is constructed by first postulating constitutive equations to be equations of state in the strain, ϵ_{kl}, temperature, T, temperature gradient, g_k, and internal state, α_{kl}^{μ}, as follows [2]:

the stress tensor:

$$\sigma_{ij} = \sigma_{ij}(\epsilon_{kl}, T, g_k, \alpha_{kl}^{\mu}) \tag{1}$$

the internal energy:

$$u = u(\epsilon_{kl}, T, g_k, \alpha_{kl}^{\mu}) \tag{2}$$

the entropy:

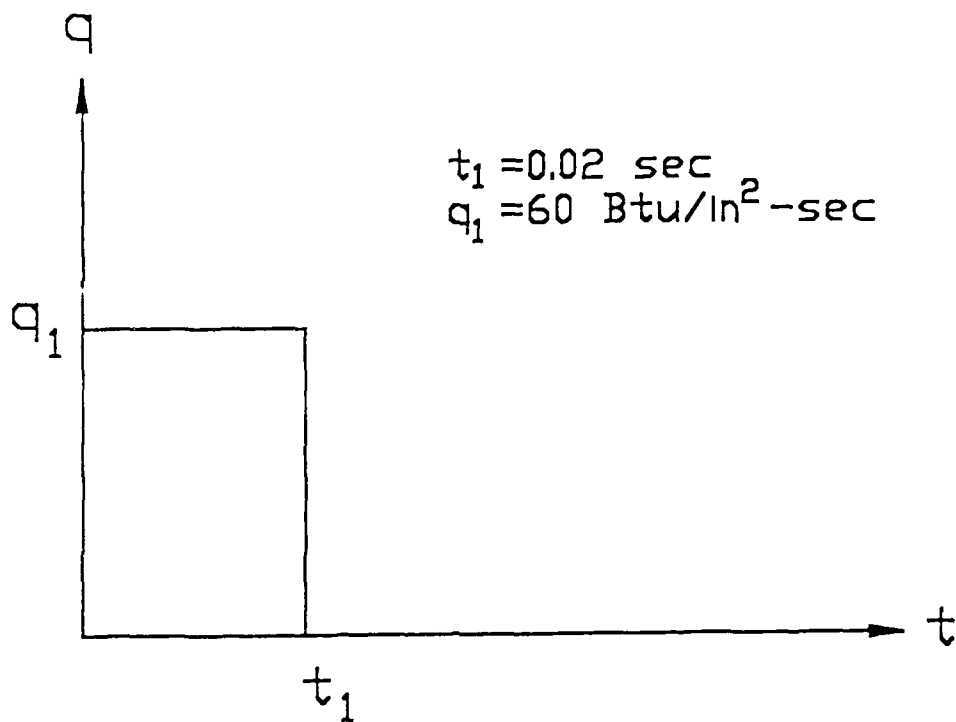$$s = s(\epsilon_{kl}, T, g_k, \alpha_{kl}^{\mu}) \tag{3}$$

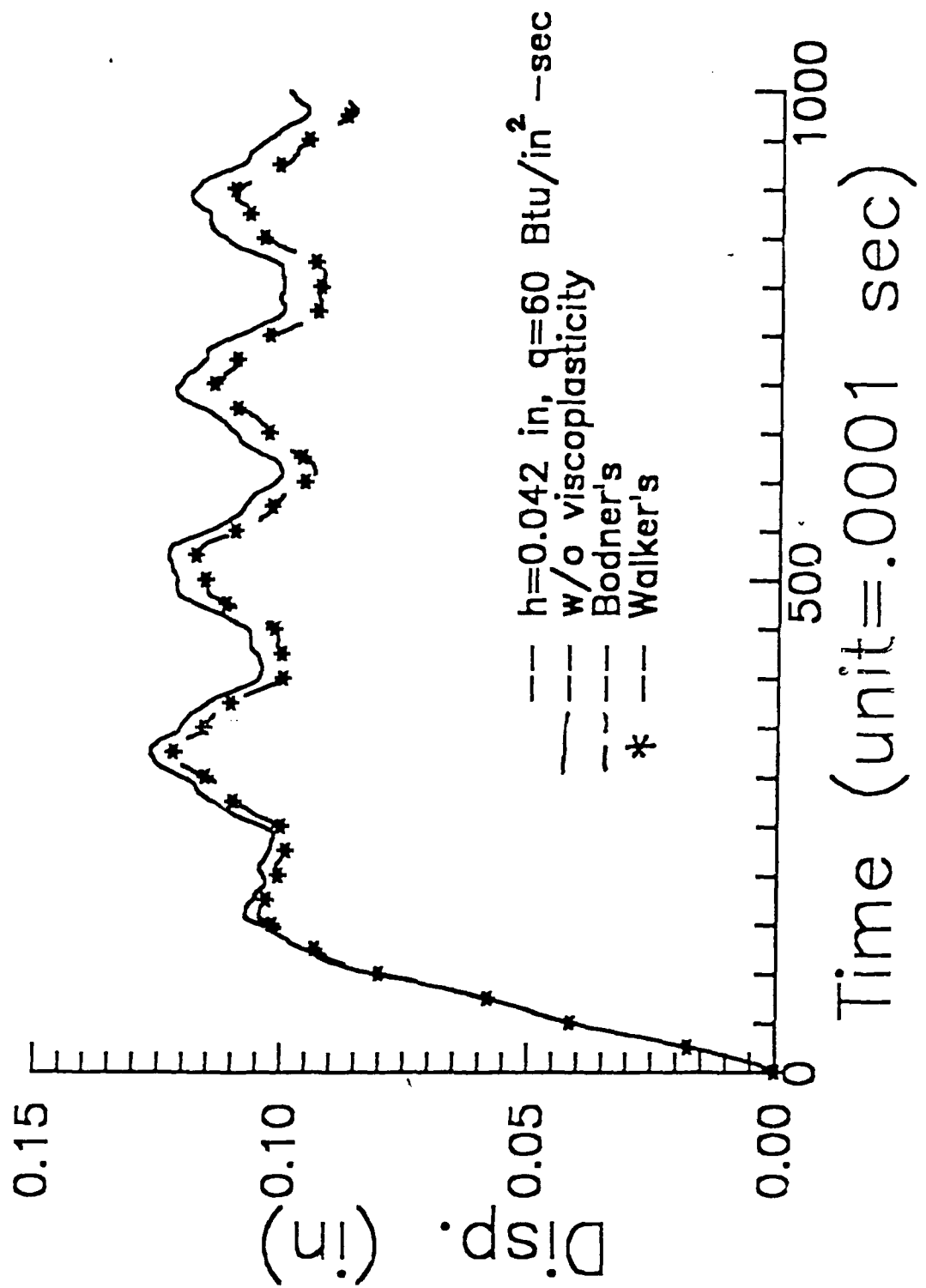Fig. 1. Heat Input for Circular Plate of Radius 10 in

5

Fig. 2.   Center Displacement Versus Time for Circular Plate with Instantaneous
Heat Input

6

Fig. 3. Displacement Profile for Circular Plate with Instantaneous Heat Input

7

Fig. 4.   Inelastic Strain Versus Time for Circular Plate with Instantaneous
Heat Input

8

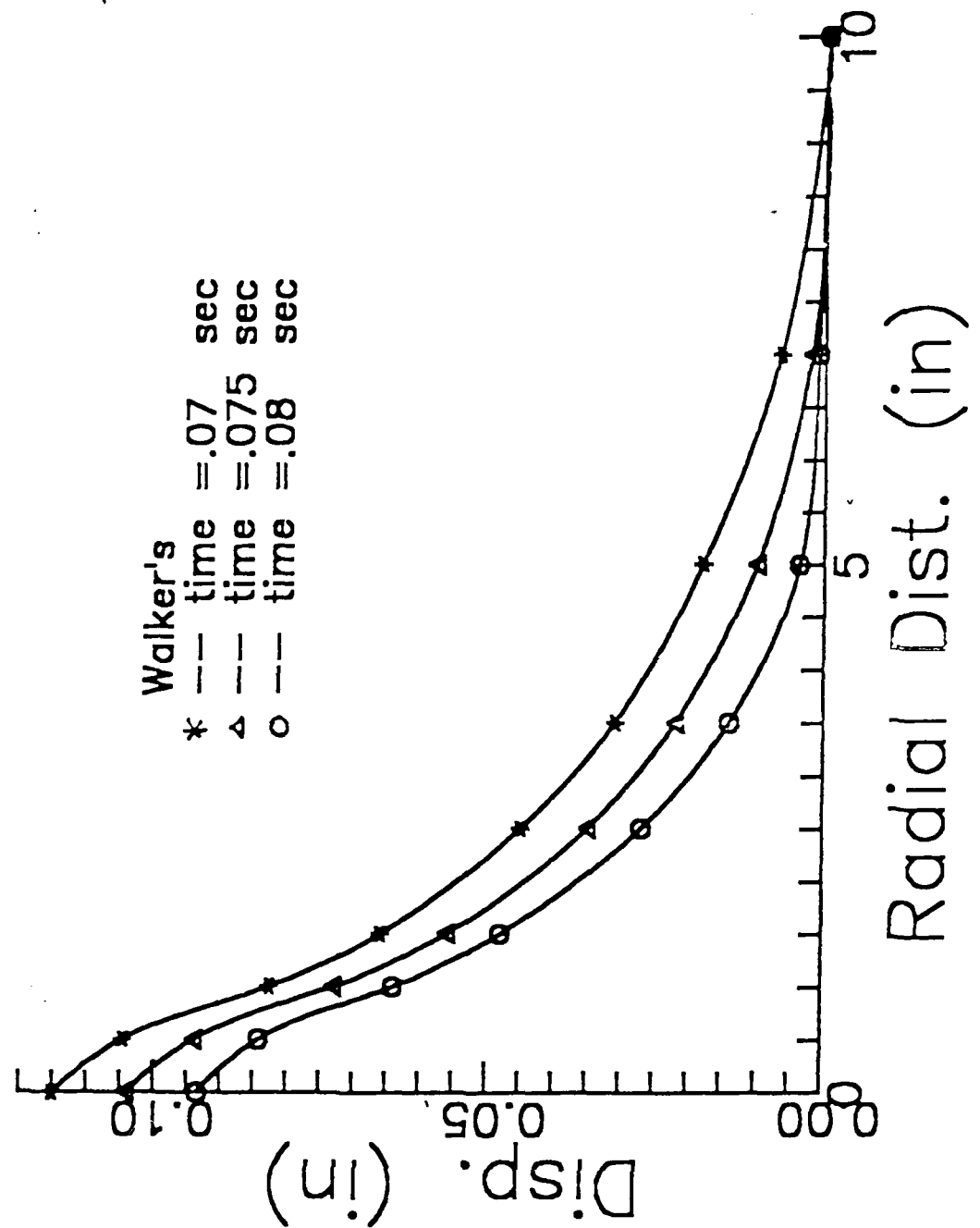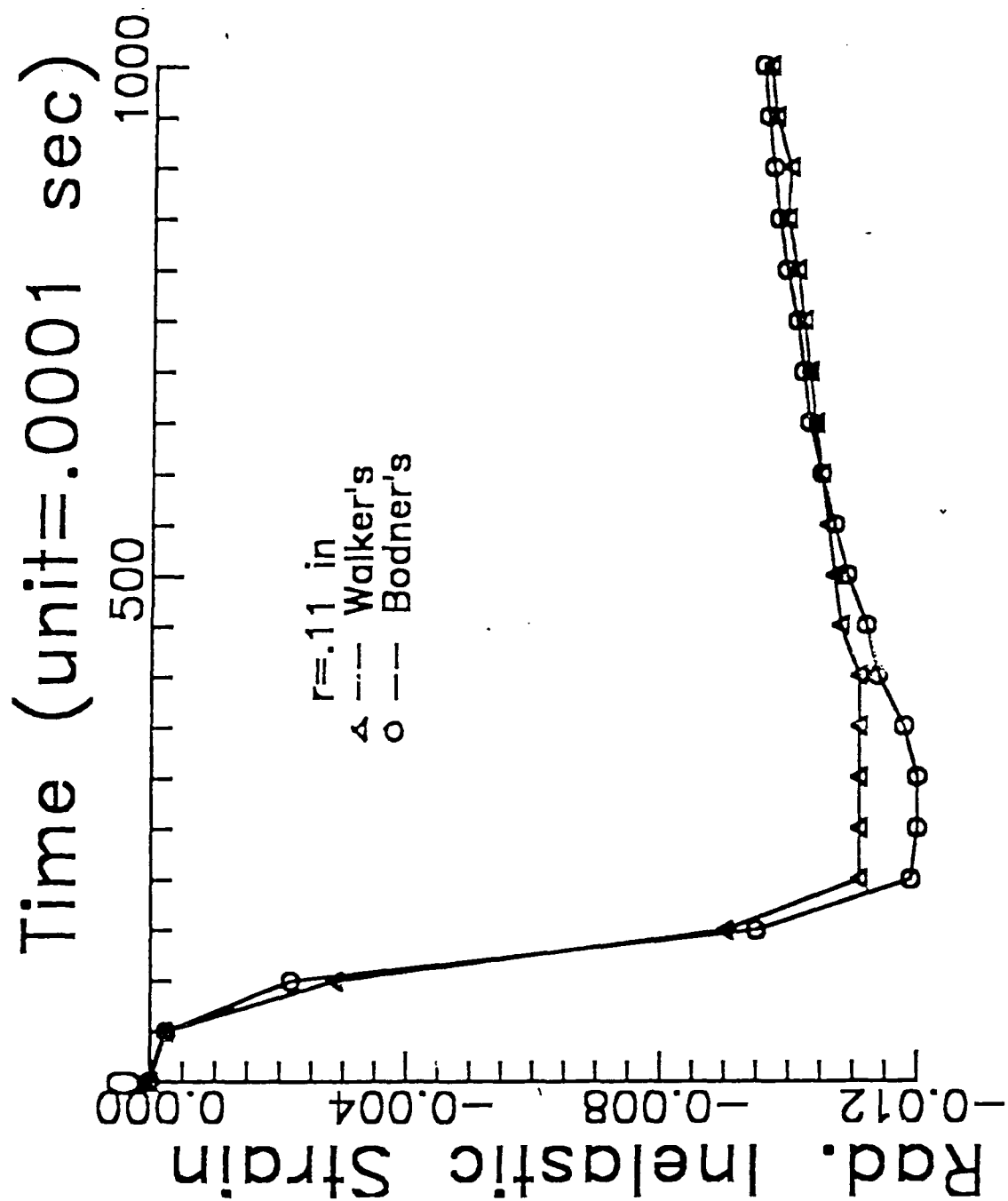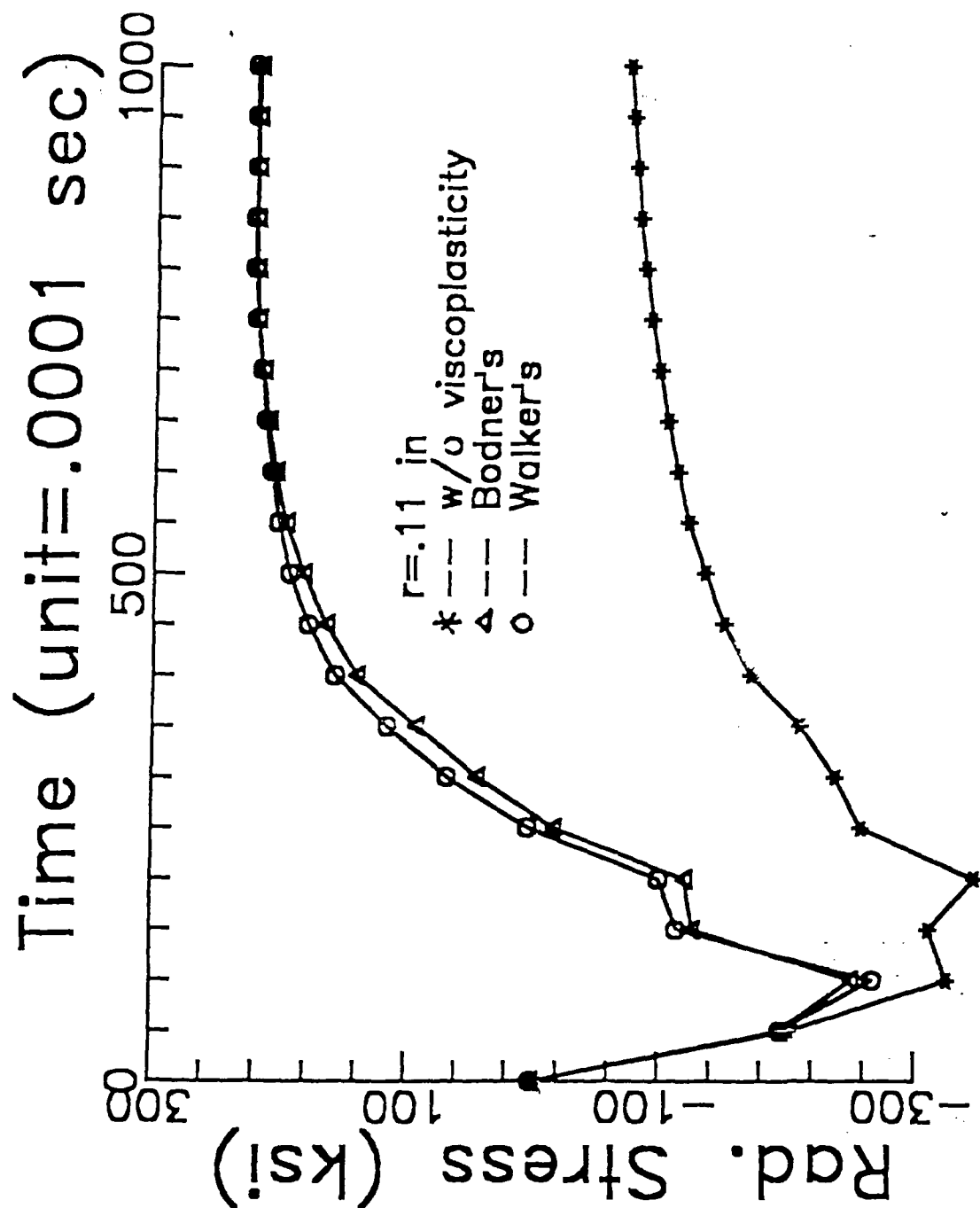Fig. 5. Radial Stress Versus Time for Circular Plate with Instantaneous
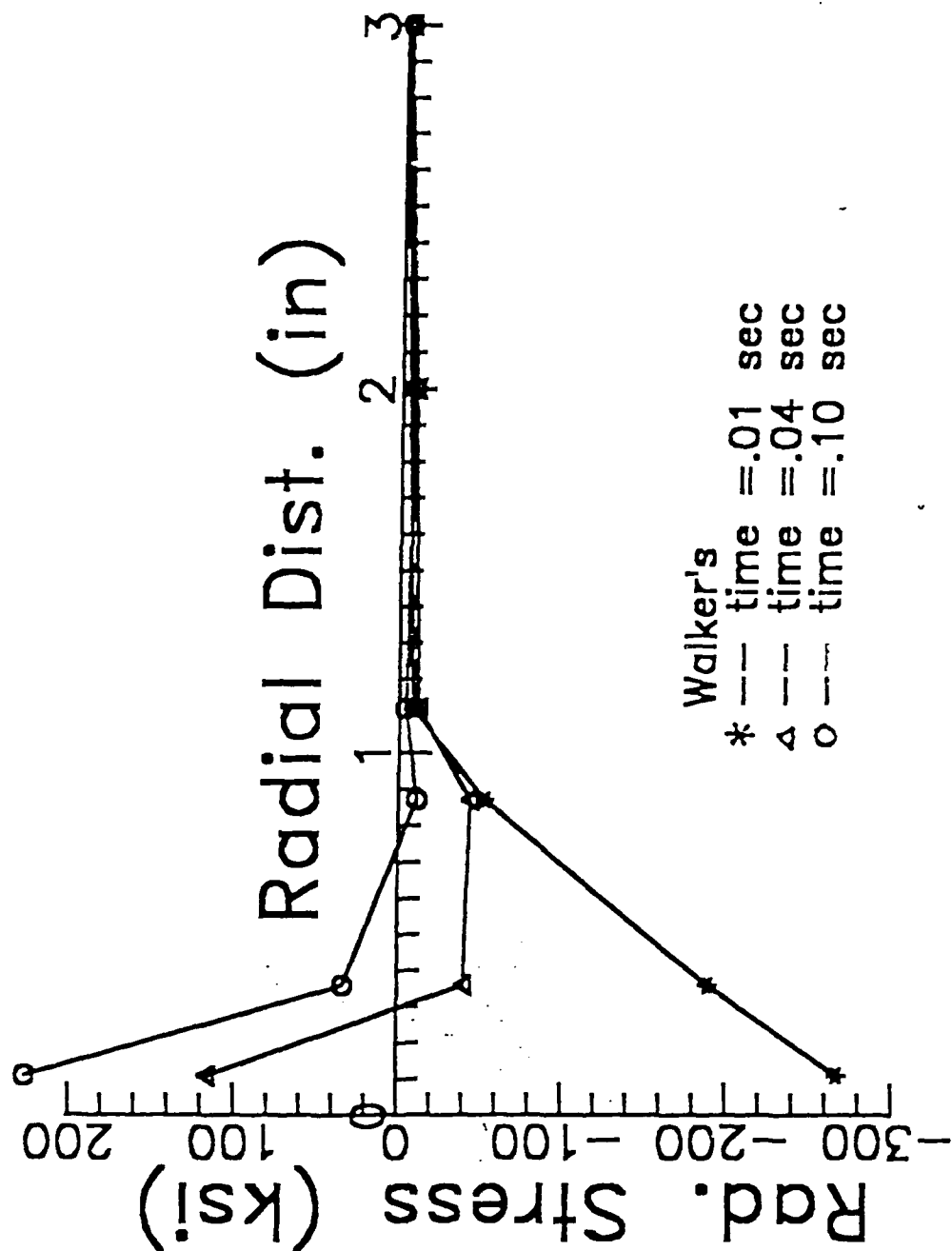Heat Input

9

Fig. 6. Radial Stress Profile for Circular Plate with Instantaneous Heat Input
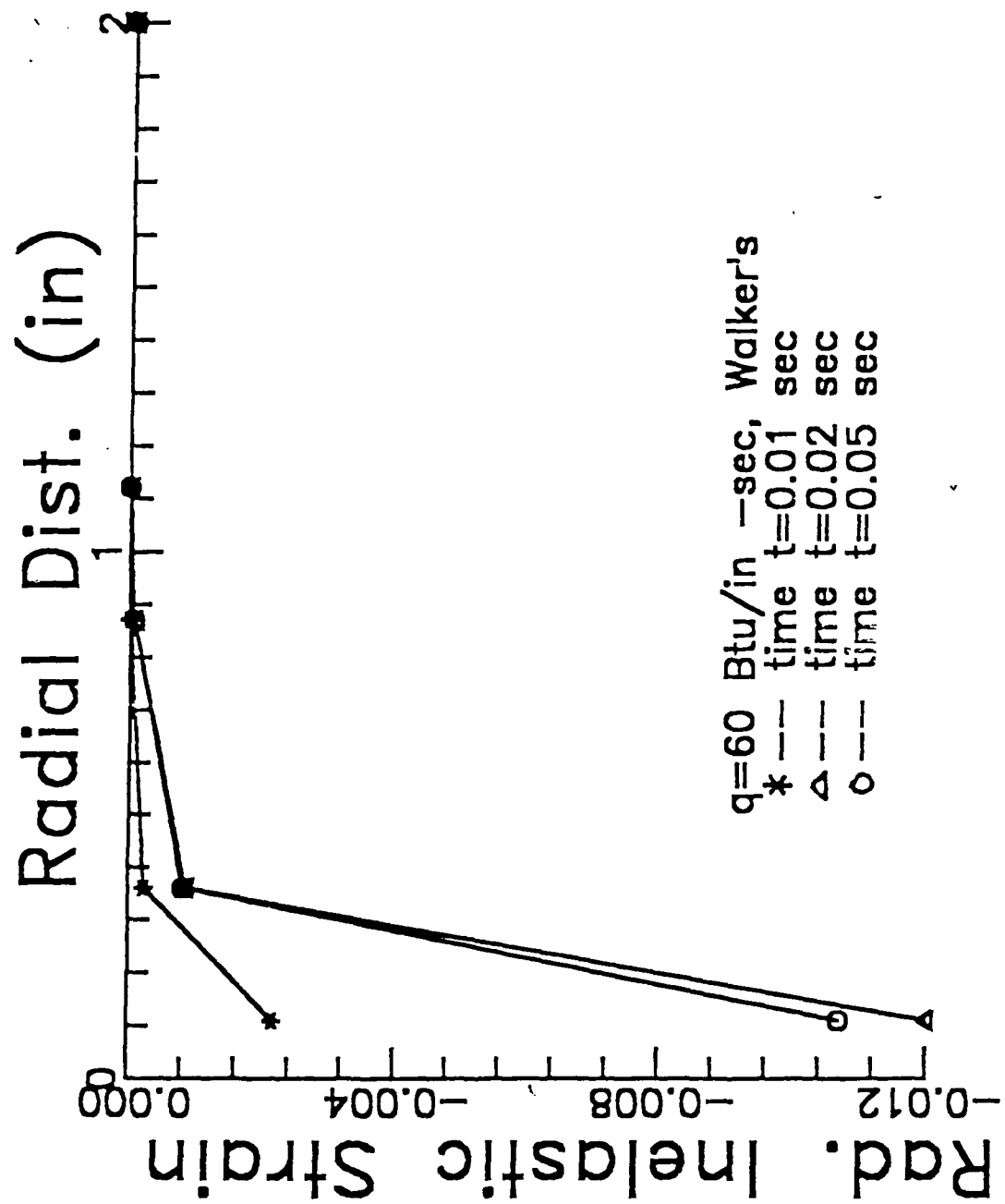
Fig. 7.   Inelastic Strain Profile for Circular Plate with Instantaneous Heat Input

11

the heat flux vector:

$$q_i = q_i(\epsilon_{kl}, T, g_k, \alpha_{kl}^\mu) \tag{4}$$

and

$$\dot{\alpha}_{ij}^\eta = \Omega_{ij}^\eta(\epsilon_{kl}, T, g_k, \alpha_{kl}^\mu, \dot{\alpha}_{kl}^\mu) \quad , \quad \eta=1,\ldots,n; \; \mu=1,\ldots,n \tag{5}$$

where α_{ij}^η are a set of n internal states variables. Now define the Helmholtz free energy

$$h = u - Ts = h(\epsilon_{kl}, T, g_k, \alpha_{kl}^\mu) \tag{6}$$

Therefore,

$$\dot{h} = \frac{\partial h}{\partial \epsilon_{kl}} \dot{\epsilon}_{kl} + \frac{\partial h}{\partial T} \dot{T} + \frac{\partial h}{\partial g_k} \dot{g}_k + \frac{\partial h}{\partial \alpha_{kl}^\mu} \dot{\alpha}_{kl}^\mu \tag{7}$$

Substituting the above into the first law of thermodynamics and this result into the second law of thermodynamics gives

12

$$\rho T \dot{s}_I = [\sigma_{ij}(\epsilon_{kl},T,g_k,\alpha_{kl}^\mu) - \rho\frac{\partial h}{\partial \epsilon_{ij}}(\epsilon_{kl},T,g_k,\alpha_{kl}^\mu)]\dot{\epsilon}_{ij}$$

$$- [\rho \frac{\partial h}{\partial T}(\epsilon_{kl},T,g_k,\alpha_{kl}^\mu) + \rho s(\epsilon_{kl},T,g_k,\alpha_{kl}^\mu)]\dot{T}$$

$$- [\rho \frac{\partial h}{\partial g_i}(\epsilon_{kl},T,g_k,\alpha_{kl}^\mu)]\dot{g}_i$$

$$- [\frac{\partial h}{\partial \alpha_{ij}^\eta}(\epsilon_{kl},T,g_k,\alpha_{kl}^\mu)]\ \Omega_{ij}^\eta(\epsilon_{kl},T,g_k,\alpha_{kl}^\mu,\dot{\alpha}_{kl}^\mu)$$

$$- [q_i(\epsilon_{kl},T,g_k,\alpha_{kl}^\mu)/T]g_i \geq 0 \qquad\qquad (8)$$

Using the Coleman-Mizel [3] procedure, it now follows that

$$\frac{\partial h}{\partial g_i} = 0 \quad => \quad h=h(\epsilon_{kl},T,\alpha_{kl}^\mu) \qquad\qquad (9)$$

By a similar argument

$$s = \frac{-\partial h}{\partial T} \quad => \quad s=s(\epsilon_{kl},T,\alpha_{kl}^\mu) \qquad\qquad (10)$$

13

Also,

$$\sigma_{ij} = \rho \frac{\partial h}{\partial \epsilon_{ij}} \implies \sigma_{ij} = \sigma_{ij}(\epsilon_{kl}, T, \alpha_{kl}^{\mu}) \tag{11}$$

Note that although the above is similar to the result obtained for elastic materials, h is no longer a potential for the stress tensor because it is path dependent due to its dependence on the internal state.

Inequality (8) now reduces to

$$\rho T \gamma = - \rho \frac{\partial h}{\partial \alpha_{ij}^{\eta}} \Omega_{ij}^{\eta} - q_i g_i / T \geq 0 \tag{12}$$

where the first term represents internal dissipation and the last term is heat conduction dissipation. Note that the internal dissipation cannot be set to zero because although the rate of change of the internal state variables may be specified, the actual internal state at any time cannot be specified.

It can also be shown that [3]

$$q_i = -k_{ij} g_j + H.O.T. \tag{13}$$

Thus, if internal state variable growth laws (5) can be determined the problem will be completely specified by construction of the Helmholtz free energy function (equation (9)).

Now consider a special case of equation (9) which is found to be suitable for many materials. Let

$$h = h(\epsilon_{kl}, T, \epsilon_{kl}^{I}) \tag{14}$$

14

where ϵ_{kl}^{I}, called the inelastic strain tensor, is equivalent to α_{kl}^{I}.

Expanding h in a second order Taylor series in its arguments gives

$$h = \frac{1}{\rho}\left[A+BT'+C_{ij}\epsilon_{ij}+\tfrac{1}{2}D_{ijkl}\epsilon_{ij}\epsilon_{kl}+E_{ij}\epsilon_{ij}^{I}+F_{ijkl}\epsilon_{ij}\epsilon_{kl}^{I}+\right.$$

$$\left.+\tfrac{1}{2}G_{ijkl}\epsilon_{ij}^{I}\epsilon_{kl}^{I}+H_{ij}\epsilon_{ij}T'+I_{ij}\epsilon_{ij}^{I}T'+\tfrac{1}{2}KT'^{2}\right] \tag{15}$$

Substituting the above into (11) results in

$$\sigma_{ij} = C_{ij}+D_{ijkl}\epsilon_{kl}+F_{ijkl}\epsilon_{kl}^{I}+H_{ij}T' \tag{16}$$

The above may be written equivalently

$$\sigma_{ij} = \sigma_{ij}^{R}+D_{ijkl}\left[\epsilon_{kl}-\epsilon_{kl}^{I}-\alpha_{kl}(T-T_{0})\right] \tag{17}$$

where σ_{ij}^{R} is the residual stress, D_{ijkl} is the linear elastic modulus tensor, and α_{kl} is the thermal expansion coefficient tensor. From (17) it is clear that

$$\epsilon_{ij}^{I} \equiv \epsilon_{ij}-\epsilon_{ij}^{E}-\alpha_{ij}(T-T_{0}) \tag{18}$$

where ϵ_{ij}^{E} is the elastic strain tensor, given by

$$\epsilon_{ij}^{E} = D_{ijkl}^{-1}(\sigma_{kl}-\sigma_{kl}^{R}) \tag{19}$$

The above equations will be shown to be suitable for characterizing the material behavior of elastic-plastic media with internal state variables.

To obtain the coupled heat conduction equation recall the first law:

$$\rho\dot{u} = \sigma_{ij}\,\dot{\epsilon}_{ij} - q_{j,j} + \rho\dot{r} \tag{20}$$

Therefore, due to definition (6) we obtain

$$\rho(\dot{h}+\dot{T}s+T\dot{s}) = \sigma_{ij}\,\dot{\epsilon}_{ij} - q_{j,j} + \rho\dot{r} \tag{21}$$

From (9) we know that

$$\dot{h} = \frac{\partial h}{\partial \epsilon_{ij}}\,\dot{\epsilon}_{ij} + \frac{\partial h}{\partial T}\,\dot{T} + \frac{\partial h}{\partial \alpha_{ij}^{\eta}}\,\dot{\alpha}_{ij}^{\eta} \tag{22}$$

Substituting (22) into (21) gives

$$- \left(\sigma_{ij} - \rho\,\frac{\partial h}{\partial \epsilon_{ij}}\right)\,\dot{\epsilon}_{ij} + \rho\left(\frac{\partial h}{\partial T} + s\right)\dot{T} + \rho T\dot{s}$$

$$+ \rho\,\frac{\partial h}{\partial g_i}\,\dot{g}_i + \rho\,\frac{\partial h}{\partial \alpha_{ij}^{\eta}}\,\dot{\alpha}_{ij}^{\eta} + q_{j,j} - \rho\dot{r} = 0 \tag{23}$$

Utilizing (9) through (11) results in

$$\rho T\dot{s} + \rho\,\frac{\partial h}{\partial \alpha_{ij}^{\eta}}\,\dot{\alpha}_{ij}^{\eta} + q_{j,j} - \rho\dot{r} = 0 \tag{24}$$

Utilizing (3) and (10) gives

16

$$\dot{S} = \frac{\partial S}{\partial \epsilon_{ij}} \dot{\epsilon}_{ij} + \frac{\partial S}{\partial T} \dot{T} + \frac{\partial S}{\partial \alpha^n_{ij}} \dot{\alpha}^n_{ij} \qquad (25)$$

Substituting (25) into (24) thus gives

$$\rho T \frac{\partial S}{\partial \epsilon_{ij}} \dot{\epsilon}_{ij} + \rho T \frac{\partial S}{\partial T} \dot{T} + \rho T \frac{\partial S}{\partial \alpha^n_{ij}} \dot{\alpha}^n_{ij} + \rho \frac{\partial h}{\partial \alpha^n_{ij}} \alpha^n_{ij}$$

$$+ q_{j,j} - \rho \dot{r} = 0 \qquad (26)$$

Utilizing (11) gives

$$- \rho T \frac{\partial^2 h}{\partial \epsilon_{ij} \partial T} \dot{\epsilon}_{ij} - \rho T \frac{\partial^2 h}{\partial T^2} \dot{T} - \rho T \frac{\partial^2 h}{\partial \alpha^n_{ij} \partial T} \dot{\alpha}^n_{ij} + \rho \frac{\partial h}{\partial \alpha^n_{ij}} \dot{\alpha}^n_{ij}$$

$$+ q_{j,j} - \rho \dot{r} = 0 \qquad (27)$$

so that substitution of (13) into the above will give

$$\rho \frac{\partial h}{\partial \alpha^n_{ij}} \dot{\alpha}^n_{ij} - \rho T \frac{\partial^2 h}{\partial \alpha^n_{ij} \partial T} \dot{\alpha}^n_{ij} - \rho T \frac{\partial^2 h}{\partial \epsilon_{ij} \partial T} \dot{\epsilon}_{ij} - \rho T \frac{\partial^2 h}{\partial T^2} \dot{T}$$

$$- (k_{ij} g_j)_{,i} - \rho \dot{r} = 0 \qquad (28)$$

Note that for an elastic material $\dot{\alpha}^n_{ij} = 0$ and the above reduces to the coupled heat conduction equation for elastic media. Since terms 1 and 2 could be large even under non-inertial conditions, they should be considered carefully in inelastic problems.

Finally, substituting (17) into the above gives

$$- D_{ijkl}(\epsilon_{kl} - \alpha_{kl}^1 + \alpha_{kl} T_0)\dot{\alpha}_{ij}^1 - D_{ijkl}\,\alpha_{ij}\,\alpha_{kl}\,T\dot{T} + D_{ijkl}\,\alpha_{ij}\,T\,\dot{\epsilon}_{kl}$$

$$+ \rho\, C_v\, \dot{T} - (k_{ij}\, g_j)_{,i} - \rho\dot{r} = 0 \tag{29}$$

The above equation is the two-way coupled heat conduction equation. Note that a change in either the state of strain, $\dot{\epsilon}_{kl}$, or the internal state, $\dot{\alpha}_{ij}^1$, has an effect on the temperature, T.

The authors have previously studied the above equation for a point mass |4| and in one dimension |5|. The inclusion of two-way coupling adds considerable complexity to the computational algorithm for solving the problem in any number of dimensions.

We are currently developing two algorithms to account for this thermomechanical coupling. In the first, we have reduced all of the field equations, including (29), to two-dimensional axisymmetric form and are utilizing continuum elements to obtain a solution for both the temperature and displacement fields.

In the second method, we are modifying the one-way coupled code previously developed by the authors [5]. We are using an operator splitting method previously proposed by Oden [6]. In this approach, the problem is solved on each time increment by assuming one-way coupling and the coupling terms are then included in the thermal analysis until iterative convergence is obtained on each time step. We hope to have one or both of these algorithms operational by June, 1989.

2.3.3 Computational Facilities Development

It was apparent from the inordinate computational times required to operate the one-way coupled code that it would be necessary to improve our

18

computational efficiency in order to develop two-way coupled algorithms [5]. Therefore, the authors have spent the last several months upgrading our computer capabilities. We have purchased a microVAX to be utilized as a dedicated machine for use with the algorithms developed as part of the current contract. This system has now been connected to the campus VAX network, and initial indications are that the computational times will be decreased somewhat. However, because the improved efficiency has not been as much as we had hoped for, we have undertaken to streamline the one-way coupled code somewhat before proceeding to implement the two-way coupling. These efficiency measures are nearing completion at this time.

2.4 Experimental Programs

The experimental program has been divided into two major categories: 1) constitutive testing of uniaxial specimens under steady state and transient temperature conditions; and 2) structural testing of plates subjected to rapid external heating. The experimental efforts are discussed in greater detail in the following two subsections.

The constitutive tests are used to evaluate the material parameters for the thermoviscoplastic constitutive models used in the structural analysis program described in Section 2.2. Currently, these models will utilize constants obtained from tests conducted at several elevated steady state temperatures. Material response at intermediate temperatures is then computed using interpolated values of the parameters. This approach may lead to erroneous predictions if the material undergoes a significant phase change during a temperature transient. To investigate this phenomenon, a set of experiments is being developed and performed which will enable us to extend

19

the current constitutive theories to predict material behavior under transient temperature conditions.

The structural testing of plates subjected to rapid external heating is being performed in order to critically compare the theory developed herein. Primary emphasis is being placed on prediction of the plate response for both temperature and displacement fields. In addition, more physical insight to the problem we are modelling is being obtained.

2.4.1 Constitutive Testing

Uniaxial constitutive experiments are currently being conducted in a steady state temperature environment in order to verify and supplement the material parameter data base obtained from [7]. Hastelloy X has been selected as the candidate material for this research primarily because of the availability of such information. Therefore, upon completion of these tests, material constants for Hastelloy X at room temperature, 1000°F, 1200°F, 1600°F, and 1800°F will be used to perform the structural analysis discussed in the previous sections.

The uniaxial specimens used for testing are standard LCF uniform-gage test section specimens, machined to ASTM specifications. Typical tests being performed include: 1) creep tests; 2) stress relaxation tests; 3) monotonic constant strain rate tests; 4) fully reversed cyclic tests; and 5) stress drop tests during monotonic and cyclic loading. All experiments are being performed at Texas A&M University using an MTS 880 electro-hydraulic testing machine and clam shell oven.

The three zone clamshell oven and closed loop control system allows for accurate temperature control in the specimen gage section with nominal spatial temperature gradients. Specimen temperature is obtained using three, contact

mounted, K-type thermocouples. While intrinsically mounted thermocouples would allow for more accurate temperature measurement, past experience has shown that this method of attachment severely degrades the fatigue life of the specimen.

Constitutive tests of uniaxial specimens under transient temperature conditions is also underway, in order to extend the validity of current models to high thermal rates. Specimens specifically designed for combined thermomechanical loading are being evaluated for this phase of testing. The specimen geometry is that of an LCF efficiency button head specimen, machined to ASTM specifications. To study the uniformity of the transverse temperature gradient, specimens have been fabricated to have either a solid or hollow core. In order to provide test to test compatibility, hastelloy-X is also being used in this phase of testing.

Another difficult aspect of transient temperature testing is minimization of the longitudinal thermal gradient during a thermal transient. A quad-elliptical quartz lamp furnace is being used and will hopefully alleviate this potential problem. Approximately thirty K-type thermocouples are being used to monitor the temperature fields in the gage section of the specimen.

In order to obtain useful information about the thermomechanical constitutive behavior of inelastic materials under transient temperature conditions, it is necessary to impose extremely complex strain histories, in addition to the thermal histories. The MTS 880 electo-hydraulic testing machine is being modified to simultaneously measure mechanical and thermal data and control (in a closed loop fashion) both aspects of the experiment. Therefore, one of the main goals of the phase of testing is to identify acceptable experimental techniques for these type of experiments.

21

2.4.2 Plate Testing

Indications from the first set of plate experiments performed at AFWAL are that the acquired data are not representative of the actual experimental output. This is believed to be due to an inordinate amount of electronic noise which masked the output produced by both the LVDT's and the thermocouples. We hypothesize at this time that this was caused by the installation of a second laser on the day that the experiments were performed. Therefore, we are currently planning to rerun the tests in the near future. At the present time, the technicians onsite are preparing the experiments and debugging the electronic data acquisition units. The second set of tests are scheduled to be performed in March.

2.5 Conclusions

There exists a need to develop models capable of predicting the response of aerospace structures to complex thermomechanical inputs which produce significant material inelasticity and resulting two-way thermomechanical coupling and to verify these models against controlled experiments.

This report documents progress made during the past six months towards achieving this goal.

2.6 References

1. Chang, H.T. and Allen, D.H., "Analysis of a Viscoplastic Plate Subjected to Rapid External Heating," to appear in _Finite Elements in Analysis and Design_, 1989 (See Appendix 6.1).

2. Coleman, B.D. and Gurtin, M.E., "Thermodynamics with Internal State Variables," _Journal of Chemical Physics_, Vol. 47, pp. 597-613, 1967.

3. Coleman, B.D. and Mizel, V.J., "Thermodynamics and Departures from Fourier's Law of Heat Conduction," _Archive for Rational Mechanics and Analysis_, Vol. 13, pp. 245-261, 1963.

4. Allen, D.H., "A Prediction of Heat Generation in a Thermoviscoplastic Uniaxial Bar," _International Journal of Solids and Structures_, Vol. 21, No. 4, pp. 325-342, 1985.

5. Allen, D.H., "Predicted Axial Temperature Gradient in a Viscoplastic Uniaxial Bar Due to Thermomechanical Coupling," _International Journal for Numerical Methods in Engineering_, Vol. 23, No. 5, pp. 903-917, 1986.

6. Oden, J.T., _Finite Elements of Nonlinear Continua_, McGraw-Hill, New York, 1972.

7. Tony, M., NASA Lewis Research Center, personal correspondence.

3.0 PUBLICATION LIST

The following papers have been accepted for publication:

1. Chang, H.T. and Allen, D.H., "Analysis of a Viscoplastic Plate Subjected to Rapid External Heating," to appear in <u>Finite Elements in Analysis and Design</u> (see Appendix 6.1).

2. Imbrie, P.K., Allen, D.H., and Chang, H.T., "Laser/Structure Interaction - A Comparison of Theory Experiment," <u>Proceedings AIAA Aerospace Sciences Meeting</u> (see Appendix 6.2).

4.0 RESEARCH ASSIGNMENTS

4.1 Faculty

1. Dr. D.H. Allen (Co-principal Investigator) - overall project coordination; development of coupled field equations; development of transient temperature constitutive equations; experimental programs; one-way coupled finite element models.

2. Dr. M.S. Pilant (Co-principal Investigator) - development of coupled field equations; two-way coupled finite element models.

3. Mr. P.K. Imbrie (Lecturer and Ph.D. Candidate) - coordinator for experimental programs; transient temperature constitutive models.

4.2 Additional Staff

1. Ms. C. Harmon (Secretary) - secretarial support.

2. Ms. L.D. McCrea (M.S. Research Assistant) - experimental constitutive equations.

3. Mr. G.Jeony (Ph.D. Candidate) - two-way coupled finite element model.

4. Mr. T. Byrom (Ph.D. Candidate) - computational solutions.

5.0 INTERACTIONS

5.1 <u>Presentations</u>

1. Allen, D.H., Imbrie, P.K., and Chang, H.T., "Analysis and Experiment of Rapidly Heated Viscoplastic Plates," ASME Winter Annual Meeting, Chicago, 1988.

2. Imbrie, P.K. and Allen, D.H., "Laser/Structure Interaction - A Comparison of Theory to Experiment," AIAA Aerospace Sciences Meeting, Reno, 1989.

5.2 <u>Other</u>

1. Dr. Allen presented a short course on thermoviscoplasticity at NASA Langley Research Center in October, 1988. This course is also to be presented immediately following the 30th SDM Conference in 1989.

6.0 APPENDIX

INTERIM TECHNICAL REPORTS

APPENDIX 6.1

Analysis of a Viscoplastic Plate
Subjected to Rapid External Heating

by

H.T. Chang
Aerostructures, Inc.
Arlington, VA. 22202

and

D.H. Allen
Aerospace Engineering Department
Texas A&M University
College Station, Texas 77843

ABSTRACT

A computational analysis is presented herein for an axisymmetric plate subjected to rapid external heating. The analysis is complicated by several forms of nonlinearity, including radiation boundary conditions, material viscoplasticity and geometric nonlinearity. The mechanical constitution is extremely complex, involving history and rate dependence which causes the constitutive equations to be mathematically stiff. Results are obtained for two viscoplasticity models available in the current literature.

The solution utilized herein adopts the finite element method in spatial coordinates and standard finite differencing in time. Iterative techniques are used to account for nonlinearity. Results are obtained for a circular plate subjected to a high energy instantaneous heat source applied axisymmetrically to one side of the plate. Sensitivity studies are conducted to determine the effects of various heat intensities and plate thicknesses on temperature, displacements, and stresses. It is found that material viscoplasticity and geometric nonlinearity contribute significantly to the predicted response of the plate.

INTRODUCTION

Plates are often subjected to rapid heating capable of producing highly nonlinear structural response. Examples are structural components subjected to laser heating, the skins of aerodynamic vehicles in hypersonic flight, and hot gas turbine engine components. Due to the elevated temperature environment encountered in these applications it is often necessary to include thermal effects in the structural analysis.

Several theoretical solutions for a heated thin plate have been reported in the literature. In most cases either classical plate theory [1,2] or large

2

deflection plate theory [3-6] was utilized to obtain linear thermoelastic solutions. In severe thermal environments, however, the plate response may become highly nonlinear. Large variations in the temperature field necessitate inclusion of temperature dependent thermal conductivity. Furthermore, the nonuniformly distributed thermal strain induces geometric nonlinearity and localized inelastic stresses. It is thus a formidable task to extend the previous solutions to account for these nonlinearities.

Recently, attempts have been made to numerically approximate the solution for a heated elastic plate [7,8] by the boundary element method. Kawakami and Shiojiro [9] attempted to implement ADINAT/ADINA with the capability of performing heat transfer analysis and thermoelastic-plastic analysis for plate/shell elements. In their research, plasticity in the element is assumed only when the cross section is totally plastic. Therefore, their solution does not apply to a plate subjected to rapid high energy heating on one surface.

The authors have reported a computational analysis for an axisymmetric viscoplastic plate subjected to rapid external heating [10]. To our knowledge this is the first plate analysis involving both heat transfer and viscoplasticity to be reported in the open literature. In this previous research it was assumed that the thermal response of the plate was independent of mechanical deformations. Thus, it was possible to obtain the heat transfer solution first and supply the results of this analysis to the mechanical solution. The finite element method was employed for spatial discretization of both the thermal and mechanical analyses, and finite differencing was used in time. Newton iteration was used on each time step to account for global nonlinearity. This nonlinearity was induced in the thermal analysis via temperature dependence of the thermal conductivity and radiation boundary

3

conditions. In the mechanical analysis nonlinearity was caused by viscoplastic constitutive behavior, which was predicted with a constitutive model introduced by Bodner and Partom [11].

In the current paper the model is extended to include geometric nonlinearity caused by large rotations. Furthermore, a viscoplasticity model proposed by Walker [12] is incorporated for comparison to results predicted by Bodner's model. The nonlinear plate formulation, which was not included in the authors' previous paper, is discussed in some detail. Finally, sensitivity studies are conducted using the algorithm to determine the effects of heating rate and plate thickness on predicted temperature, displacements, and stresses.

MODEL DEVELOPMENT

The procedure utilized to solve the current problem is similar to that used in other simpler mechanical field problems. Therefore, the model is presented only in abbreviated form in this section. Further details of this development can be found in references [10] and [13].

A pivotal assumption in the analysis is that the heat transfer does not depend on the mechanical deformations. It is well-known that in dynamic problems this coupling may be significant even when the deformations are elastic [14]. In the case of inelastic response such as is considered herein, this coupling may be even more substantial [15]. However, the inclusion of this term in the heat transfer analysis adds considerable complexity to the computational scheme [15]. Therefore, since in the examples considered herein the external source is several orders of magnitude larger than the internal heat generation, the authors have neglected the mechanical coupling in the heat transfer solution. This issue is planned to be the thrust of future research by the authors on this subject.

4

As shown in Fig. 1, due to the uncoupling assumption the solution algorithm may be constructed in two stages for each time step. First, the temperature field is evaluated by using finite elements in spatial coordinates and the Crank-Nicholson scheme in time. Nonlinearity due to temperature dependent thermal conductivity and radiation boundary conditions is accounted for via Newton iteration. The resulting temperature distribution is then passed to the mechanical problem as input, and the mechanical solution is obtained by using plate elements in conjunction with the Newmark-Beta method in time. Nonlinearity caused by inelastic deformations and large rotations is accounted for by Newton iteration. This procedure is performed recursively to march forward for the desired time span. The solution scheme is described in further detail below.

Thermal Analysis

An axisymmetric finite element model, developed to include nonlinear radiation boundary conditions, is used to construct the temperature field as a function of r and z for each time step. A typical two-dimensional axisymmetric mesh for the thermal analysis is shown in Fig. 2.

The governing heat transfer equations are as follows:

$$\rho C_p r \frac{\partial T}{\partial t} - \frac{\partial}{\partial r}(k\ r\ \frac{\partial T}{\partial r}) - \frac{\partial}{\partial z}(k\ r\ \frac{\partial T}{\partial z}) = 0 \quad \text{in } \Omega \tag{1}$$

$$k\ r\ \frac{\partial T}{\partial r}\ n_r + k\ r\ \frac{\partial T}{\partial z}\ n_z = \bar{q}\alpha r + \varepsilon\sigma r(T_r^4 - T^4) \quad \text{on } \Gamma \tag{2}$$

where T is the temperature, ρ is the mass density, C_p is the specific heat capacity, k is the thermal conductivity, and r and z are cylindrical coordinates, as shown in Fig. 2. Also, q is the heat flux input, $\bar{\alpha}$ is the

5

thermal absorptivity, ϵ is the thermal emissivity, σ is Boltzman's constant, T_r is the reference temperature at which radiation is zero, and n_r and n_z are components of a unit outer normal vector. Finally, Ω is the interior of the domain and Γ is the boundary of the domain.

Equations (1) and (2) may be cast into a Galerkin finite element formulation |16|. Since this part of the model exists in the open literature |16|, it is not covered in detail here.

The resulting element equations are of the form

$$c_{ij}\dot{T}_j + a_{ij}T_j = q_i \tag{3}$$

where

$$c_{ij} = \int_{A_e} \rho C_p N_i N_j r dA_e \tag{4a}$$

$$a_{ij} = \int_{A_e} \left(\frac{\partial N_i}{\partial r} rk \frac{\partial N_j}{\partial r} + \frac{\partial N_i}{\partial z} rk \frac{\partial N_j}{\partial z}\right) dA_e + \int_{\Gamma_e} N_i (N_k T_k)^3 N_j r d\Gamma \tag{4b}$$

$$q_i = \int_{\Gamma_e} N_i \bar{q} r d\Gamma + \int_{\Gamma_e} N_i \sigma T_r^4 r d\Gamma_e \tag{4c}$$

Also, N_i are the finite element shape functions, A_e is the area of the element, and Γ_e is the boundary of the element. A linear triangular (three node) axisymmetric element is used in the analysis. Equation (3) for each element is assembled to give the following global system of ordinary differential equations:

$$[C]\ \{\dot{T}\} + [A]\ \{T\} = \{Q\} \tag{5}$$

The Crank-Nicholson scheme is then applied temporally to obtain the temperature field with time |17|.

Structural Analysis

In the structural analysis, Von Karman theory is assumed for the thin plate bending motion [18], and material nonlinearity and viscoplastic constitution are included in the model. The material nonlinearity is introduced via the inelastic strain tensor, ϵ_{ij}^I, which is described in the next section.

The strain components, ϵ_{ij}, are defined by

$$\epsilon_{ij} = \epsilon_{ij}^0 + z\kappa_{ij} = \frac{1}{2}(u_{i,j} + u_{j,i}) + \frac{1}{2}(u_{3,i}u_{3,j}) + z\kappa_{ij} \quad i,j = 1,2 \quad (6)$$

where ϵ_{ij}^0 are the midsurface strain components, u_i are the displacement components, and κ_{ij} are the midsurface rotation components. The constitutive relations are given by

$$\sigma_{ij} = D_{ijk\ell}(\epsilon_{ij}^0 + z\kappa_{ij} - \epsilon_{ij}^I - \epsilon_{ij}^T) \quad (7)$$

where σ_{ij} is the stress tensor, $D_{ijk\ell}$ is the elastic modulus tensor, and ϵ_{ij}^T are the components of the thermal strain tensor. Utilizing the above in a standard laminate scheme will result in

$$\left\{ \begin{array}{c} N \\ M \end{array} \right\} = \left[\begin{array}{cc} \overline{A} & \overline{B} \\ \overline{B} & \overline{D} \end{array} \right] \left\{ \begin{array}{c} \epsilon^0 - \epsilon^I - \epsilon^T \\ \kappa \end{array} \right\} \quad (8)$$

where

$$(\overline{A}_{ij}, \overline{B}_{ij}, \overline{D}_{ij}) = \int_{-\frac{h}{2}}^{\frac{h}{2}} D_{ij}(1,z,z^2) \, dz \quad (9)$$

7

and h is the plate thickness. Note that the coupling matrix $[\bar{B}]$ does not disappear due to the through-thickness variation of elastic modulus, D_{ij}, which is temperature dependent.

The governing equations for the plate motion are thus derived by satisfying the conservation of linear and angular momentum [19]:

$$N_{x,x} + N_{yx,y} - \rho u_{,tt} = 0 \tag{10}$$

$$N_{xy,x} + N_{y,y} - \rho v_{,tt} = 0 \tag{11}$$

$$[\bar{D}_{1j}\kappa_j + \bar{B}_{1j}(\epsilon_j^O - \epsilon_{ij}^I - \epsilon_j^T)]_{,xx} +$$

$$[D_{2j}\kappa_j + B_{2j}(\epsilon_j^O - \epsilon_j^I - \epsilon_j^T)]_{,yy} +$$

$$2[\bar{D}_{3j}\kappa_j + \bar{B}_{3j}(\epsilon_j^O - \epsilon_j^I - \epsilon_j^T)]_{,xy} +$$

$$p + N_x w_{,xx} + 2N_{xy} w_{,xy} + N_y w_{,yy} - \rho w_{,tt} = 0 \tag{12}$$

Integrating equations (10) through (12) against variations in the components of the displacement field will result in the following variational principle.

$$\int_A \delta u \{N_{x,x} + N_{yz,y} - \rho u_{,tt}\} \, dxdy +$$

$$\int_A \delta v \{N_{xy,x} + N_{y,y} - \rho v_{,tt}\} \, dxdy +$$

$$\int_A \delta w \{[\bar{D}_{1j}\kappa_j + \bar{B}_{1j}(\epsilon_j^O - \epsilon_{ij}^I - \epsilon_j^T)]_{,xx} +$$

$$[D_{2j}\kappa_j + \bar{B}_{2j}(\epsilon_j^O - \epsilon_j^I - \epsilon_j^T)]_{,yy} +$$

8

$$2[\overline{D}_{3j}\kappa_j + \overline{B}_{3j}(\epsilon_j^o - \epsilon_j^I - \epsilon_j^T)]_{,xy} + p+$$

$$N_x w_{,xx} + 2N_{,xy} + N_y w_{,yy} - \rho w_{,tt}\} \, dxdy = 0 \tag{13}$$

where N_x, N_y, and N_{xy} are components of the plate midsurface forces per unit length, u and v are the in-plane displacement components, w is the out-of-plane displacement component, and p is the out-of-plane traction.

Incrementing the field variables, neglecting the third and higher order terms of the displacement increment, and applying finite element discretization results in

$$[M] \{\ddot{u}\}^{t+\Delta t} + [K] \{\Delta u\} = \{R\}^{t+\Delta t} - \{F_1\} - \{F_2\} \tag{14}$$

where [M] is the mass matrix and

$$[K] = [K_{NL}] + [K_L] \tag{15}$$

Also,

$$[K_L] = \sum_{n=1}^{n_e} \int_{V_e} [B_{NL}]^{TR} [D]^{t+\Delta t} [B_L] \, dV_e \tag{16}$$

$$[K_{NL}] = \sum_{n=1}^{n_e} \int_{V_e} [B_{NL}]^{TR} [S]^{t+\Delta t} [B_{NL}] \, dV_e \tag{17}$$

where $[B_L]$ and $[B_{NL}]$ are the linear and nonlinear strain deformation mapping matrices, respectively. Also, $\{R\}$ is the external load vector and

9

$$\{F_1\} = \sum_{n=1}^{n_e} \int_{V_e} [B_L]^{TR} (\{o\} - [D]^{t+\Delta t} \{\Delta\epsilon^I + \Delta\epsilon^T\} +$$

$$[\Delta D] \{\epsilon^0 + z\kappa - \epsilon^T - \epsilon^I\}) \, dV_e \qquad (18)$$

$$\{F_2\} = \sum_{n=1}^{n_e} \int_{V_e} [B_{NL}]^{TR} (-[D]^{t+\Delta t} \{\Delta\epsilon^I + \Delta\epsilon^T\} +$$

$$[\Delta D] \{\epsilon^0 + z\kappa - \epsilon^T - \epsilon^I\}) \, dV_e \qquad (19)$$

and n_e is the number of nodes per element.

Solving equation (14) by the Newmark integration scheme will give the first approximation of $\{\Delta u\}$ at time $t+\Delta t$. The Newton iteration method will give convergence to the nonlinear solution [10,20]. The authors are currently utilizing a three-node plate element with five degrees of freedom per node, as described in references [13] and [21]. We have not employe an axisymmetric plate element because we prefer to maintain the flexibility to solve nonaxisymmetric problems.

Thermomechanical Constitutive Models

In order to prescribe the forcing functions $\{F_1\}$ and $\{F_2\}$ defined in equations (18) and (19) it is necessary to determine the inelastic strain increment, $\Delta\epsilon_{ij}^I$. This is accomplished by integration of the selected viscoplastic constitutive model. The authors are currently using Walker's model [12], as well as the anisotropic hardening form of Bodner's model [22]. These models are compared critically in reference [23].

Bodner's model assumes

$$\dot{\epsilon}_{ij}^I = \lambda o_{ij}' \qquad (20)$$

10

where σ'_{ij} is the deviatoric stress tensor, whereas Walker's model proposes

$$\dot{\epsilon}^I_{ij} = \lambda(\sigma'_{ij} - \alpha_{2ij}) \tag{21}$$

where

$$\lambda = \lambda(\sigma_{ij}, \alpha_1, \alpha_{2ij}) \tag{22}$$

and α_1 is the drag stress, and α_2 is the back stress tensor. The above is supplemented by an additional set of evolution laws of the form

$$\dot{\alpha}^\eta_{ij} = \Omega_{ij}(\sigma_{k\ell}, \alpha^\mu_{k\ell}, T) \tag{23}$$

Equations (20) and (23) are typically numerically stiff, so that numerical integration to obtain ϵ^I_{ij} is not straightforward [24]. Bodner's model is currently being integrated using Euler's forward method, whereas Walker's model is integrated using Euler's backward method [25]. Both models are subincremented within each integration point on each time step in order to produce accurate values for $\Delta\epsilon^I_{ij}$ on each global time increment.

Example Problems

To demonstrate the use of the algorithm, an isotropic circular plate with thickness h=0.042 in and radius r=10 in is selected. The material used is B1900+Hf which is a nickel-based superalloy commonly used in hot gas turbines. Material constants for Bodner's and Walker's models are shown in Tables 1 and 2, respectively. The thermal boundary conditions are of radiation type with reference temperature T_R=0°F on all boundaries including the plate edge at r=10 in. An instantaneous heat flux is assumed to be evenly

11

distributed over a spot of radius 0.5 in at the center of the plate. All components of the displacements and rotations are assumed to be zero at the plate edge r=10 in.

The finite element mesh diagrams for the thermal and structural analyses are shown in Fig. 2. Although a fairly coarse mesh was utilized, more refined meshes showed that the global thermal and structural responses were not significantly compromised by using the current mesh. The number of global degrees of freedom was held to a minimum because the nonlinear examples presented herein required approximately 15 hours of CPU time on a VAX/8800. This is due to the fact that the global nonlinearity necessitated the use of very small time steps. In the examples shown herein, the maximum allowable time step was 0.00001 sec, thus resulting in a total of 1500 time steps.

Figure 3 shows the predicted transverse deflection at the center of the plate for a heat flux of 60 Btu/in^2-sec. Shown in the figure are both the geometrically linear and nonlinear results obtained by assuming the plate is linear elastic. The transverse deflection is significantly decreased by the inclusion of the nonlinear terms in equation (6), which demonstrates the importance of including geometric nonlinearity in this model. Figure 4 shows the through-thickness temperature variation at the center of the plate for various times. It is apparent that a rather large temperature gradient occurs at short times, and this through-thickness variation is the primary source of bending in the structure. Figure 5 depicts the temperature as a function of time on the plate upper surface both at the center of the plate and at r=0.5 in. From this figure it is apparent that a large in-plate temperature gradientoccurs near the center of the plate at short times. This gradient is the chief contributor to the extension of the structure.

12

Figures 6 through 10 are the results for an instantaneous heat flux of 90 Btu/in^2-sec including both geometric nonlinearity and the viscoplasticity models. As shown in Fig. 6, when the inelastic material response is included, the deflection of the center of the plate is reduced by only a small amount. However, as Fig. 7 shows, the radial stress history near the center of the plate (r=0.11 in) and on the top surface is significantly reduced by the accumulated inelastic strain. Thus, material inelasticity significantly affects the predicted stresses in the analysis. Figure 8 shows the stress history predicted by Walker's model at various positions on the top surface of the plate. Note that within the radius of the input heat flux the radial stress attains a maximum near the ultimate uniaxial strength of the material and then decreases, due to the large thermal gradient produced through the thickness. Figures 9 and 10 show the radial stress and hoop stress distributions at time t=0.01 sec on the top surface of the plate. Both components of stress are significantly reduced near the center of the plate by the accumulated inelastic strain. Figure 11 shows the in-plane deformation and Fig. 12 shows the accumulated inelastic strain at time t=0.01 sec. The inelastic strain is essentially zero for r>1 in, implying that outside this range the plate response is elastic. Also, Walker's model tends to accumulate more inelastic response than Bodner and Partom's, thus predicting slightly lower stress.

Figures 13 through 16 show the results for plates with varying thickness and identical external heating. Figure 13 shows the deflection history at the center of the plate as a function of plate thickness. The center deflection rate increases significantly with decreasing plate thickness. Figure 14 shows the radial stress at r=0.11 in on the top surface of the plate for various plate thicknesses. Although the radial stress peaks earlier with increasing

plate thickness the value of this maximum does not change dramatically. Figure 15 shows the accumulated inelastic strain at time t=0.01 sec for various plate thicknesses. Figure 16 shows the temperature rise as a function of time at the center of the plate on the upper surface. It can be seen that extremely large heat fluxes such as those considered herein will eventually cause localized ablation which cannot be handled by the current model.

Figures 17 through 20 show the results for plates with fixed thickness and various external heating rates. Figure 17 shows that increasing the heat flux produces modest changes in the center deflection rate. Figure 18 shows the radial stress history at r=0.11 in. Although slightly larger compressive peak stress is predicted, the time at which this peak occurs increases substantially with decreased heating rate. Fig. 19 shows the radial stress distribution at time t=0.01 sec for different external heating rates. Finally, Fig. 20 depicts the temperature rise on the upper surface at the center of the plate for various heating rates. As expected, the temperature rise increases substantially with heating rate.

14

CONCLUSION

In this paper, the author's previous research [10] has been extended to include large deflection plate theory and Walker's viscoplasticity model. Studies have been carried out to investigate the structural response of a thin plate subjected to rapid external heating. Several conclusions can be made from the current results. First, due to the thermally induced large stresses, the transverse deflection of the thin plate is significantly decreased if large rotations are considered. This indicates the importance of including nonlinear geometric effects in the current model. Second, the comparison studies show that while the two viscoplastic constitutive models predict approximately equivalent effects on the structural response the affects of viscoplasticity are substantial and therefore cannot be neglected. However, Walker's model tends to accumulate larger inelastic strain, which in turn predicts lower stress in the structural response.

Results indicate that the deflection rates are increased with decreasing plate thickness. Furthermore, the model accumulates greater inelastic strains with decreasing thickness. Finally, when the plate thickness is not changed, the displacement increases with increasing heating rate. In this case, only slightly greater peak compressive stresses are predicted, but the peak stress occurs more rapidly with increasing heating rate.

ACKNOWLEDGMENT

REFERENCES

1. Reisman, H. and Malone, D.P., "Laser Induced Thermoelastic Response of Circular Plate," Solid Mech. Arch. 5, Vol. 5, pp. 253-323, 1980.

2. Cheboturevskii, Y.V. and Yangubova, O.A., "Bending of a Circular Plate Heated by Linear Internal Impulse Heat Sources," Sov. Appl. Mech., Vol. 21, pp. 964-969, 1985.

3. Pal, M.C., "Large Deflection of Heated Circular Plates," ACTA Mechanica Vol. 8, pp. 82-103, 1969.

4. Pal, M.C., "Static and Dynamic Non-linear Behavior of Heated Orthotropic Circular Plate," Int. J. Non-linear Mech., Vol. 22, pp. 489-504, 1973.

5. Banerjee, B. and Datta, S., "A New Approach to an Analysis of Large Deflections of Thin Elastic Plates," Int. J. Non-linear Mech. Vol. 16, pp. 47-52, 1981.

6. Sinharay, G.C. and Banerjee, B., "A Modified Approach to Large Deflection Analyses of Thin Elastic Plates Under Thermal Loading," Mech. Res. Comun., Vol. 12, pp. 319-325, 1985.

7. Kamiya, N., Sawaki, Y., Nakamura, Y., and Fukui, A., "An Approximate Finite Deflection Analysis of a Heated Elastic Plate by The Boundary Element Method," App. Math. Modeling, Vol. 6, pp. 23-27, 1982.

8. Irschik, H., "A Boundary Integral Equation Method for Thermal Bending of Plates," Ingenieur-Archiv, Vol. 53, pp. 97-207, 1983.

9. Kawakami, M. and Shiojiro, M., "Thermo-Elastic-Plastic Analysis with a Plate/Shell Element Using ADINAT/ADINA," Computers & Structures, Vol. 21, pp. 165-177, 1985.

10. Chang, H.T. and Allen, D.H., "A Finite Element Analysis of a Viscoplastic Plate Subjected to Rapid Heating," to appear in Mechanics of Structures and Machines an International Journal, 1988.

11. Bodner, S.R. and Partom, Y., "Constitutive Equations for Elastic-Viscoplastic Strain-Hardening Materials," Journal of Applied Mechanics, Vol. 42, No. 2, pp. 385-389, 1975.

12. Walker, K.P., "Representation of Hastelloy-X Behavior at Elevated Temperature with a Functional Theory of Viscoplasticity," ASME J. Eng. Mat. & Tech., 1982.

13. Chang, H.T., "A Finite Element Model for Predicting Nonlinear Thermomechanical Response of Plate Structures to Rapid External Heating," Texas A&M University, Ph.D. Dissertation, August 1988.

14. Boley, B.A. and Weiner, J.H., Theory of Thermal Stresses, Wiley, New York, 1960.

15. Allen, D.H., "Predicted Axial Temperature Gradient in a Viscoplastic Uniaxial Bar Due to Thermomechanical Coupling," *Int. J. for Numerical Methods Engr.*, Vol. 23, No. 5, pp. 903-917, 1986.

16. Lutz, J.D., Allen, D.H., and Haisler, W.E. "A Finite Element Model for the Thermoelastic Analysis of Large Composite Space Structures," *Journal of Spacecraft and Rockets*, Vol. 24, No. 5, pp. 430-436, 1987.

17. Moshaiov, A. and Vorus, W.S., "Elastic-Plastic Plate Bending Analysis by a Boundary Element Method with Initial Plastic Moments," *Int. J. Solids Structures*, Vol. 22, pp. 1213-1229, 1986.

18. Timoshenko, S.P. and Woinowsky-Krieger, S., *Theory of Plates and Shells*, McGraw-Hill, New York, 1959.

19. Ashton, J.E. and Whitney, J.M., *Theory of Laminated Plates*, Technomic, Connecticut, 1970.

20. Bathe, K.J., *Finite Element Procedures in Engineering Analysis*, Prentice-Hall, Englewood Cliffs, 1982.

21. Batoz, J.L., Bathe, K.J., and Ho, L.W., "A Study of Three-Node Triangular Plate Bending Elements," *Int. J. Numer. Methods Engng.*, Vol. 15, pp. 1771-1812, 1980.

22. Chan, K.S., Lindholm, U.S., Bodner, S.R., and Walker, K.P., "A Survey of Unified Constitutive Theories," *Non-Linear Constitutive Relations for High Temperature App. - 1984*, NASA CP 2369, pp. 1-24, 1985.

23. James, G.H., Imbrie, P.K., Hill, P.S., Allen, D.H., and Haisler, W.E., "An Experimental Comparison of Current Viscoplastic Models at Elevated Temperature," *J. Engr. Mat. Tech.*, Vol. 109, pp. 130-139, 1987.

24. Imbrie, P.K., James, G.H., Hill, P.S., Allen, D.H., and Haisler, W.E., "An Automated Procedure for Material Parameter Evolution and Uncertainity Analysis for Viscoplastic Constitutive Models," to appear in *J. Engr. Mat. Tech.*, 1988.

25. Haisler, W.E. and Imbrie, P.K., "Numerical Considerations in the Development and Implementation of Constitutive Models," NASA CP 2369, NASA Lewis Research Center, pp. 169-186, 1985.

26. Lindholm, U.S., Chan, K.S., Bodner, S.R., Weber, R.M., Walker, K.P., and Cassenti, B.N., "Constitutive Modeling for Isotropic Materials," Second Annual Report, NASA CR-174980, July, 1985.

17

Table 1. Bodner's Constants for B1900+Hf [26]

Temperature-Independent Constants

$M_1 = .270 \ \text{Mpa}^{-1}$

$M_2 = 1.52 \ \text{Mpa}^{-1}$

$\alpha_1 = 0.0$

$Z_1 = 3000 \ \text{Mpa}$

$Z_3 = 1150 \ \text{Mpa}$

$r_1 = r_2 = 2$

$D_0 = 1 \times 10^4 \ \text{sec}^{-1}$

Temperature-Dependent Constants

Temp (C)	n	Z_0(Mpa)	$A_1 = A_2$ (sec^{-1})	$Z_2 = Z_c$(Mpa)
760	1.055	2700	0	2700
871	1.03	2400	.0055	2400
982	0.850	1900	.02	1900
1093	0.70	1200	.25	1200

Table 2. Walker's Constants for B1900+Hf [26]

Temp (C)	D(Mpa))	ν	K_1(Mpa)	B(Mpa)	η_2(Mpa)	η_3
21	1.900E5	.322	12.4	1.73E11	2.41E6	4794
427	1.900E5	.328	12.4	1.73E11	2.41E6	4794
538	1.900E5	.331	12.4	1.73E11	2.41E6	4794
649	1.800E5	.334	12.4	3.862E10	8.27E5	1714
760	1.655E5	.339	13.8	2.55E10	8.27E5	1880
871	1.438E5	.324	16.6	5.50E11	2.36E5	621.1
982	1.249E5	.351	13.8	4.20E10	9.65E4	400
1093	1.161E5	.351	9.	5.57E9	2.36E4	278.7

Temp (C)	η_4	η_5	η_6	η_9	η_{10}	η_{11}(Mpa)
21	0	.3117	0	11.87	0	4.7E3
427	0	.3117	0	11.87	0	4.7E3
538	0	.3117	0	11.87	0	4.7E3
649	0	.3117	0	16.64	0	4.7E3
760	0	.3117	C	19.83	2.44E-3	4.7E3
871	0	.3117	8.73E-4	59.33	2.44E-3	9.65E2
982	0	.3117	4.29E-4	136.	2.44E-3	0
1093	0	.3117	4.83E-2	136.	2.44E-3	0

Fig.1 Flowchart of Solution Algorithm

20

Y

Structural Analysis

X

Z

Thermal Analysis

.5'

q

h

R

10'
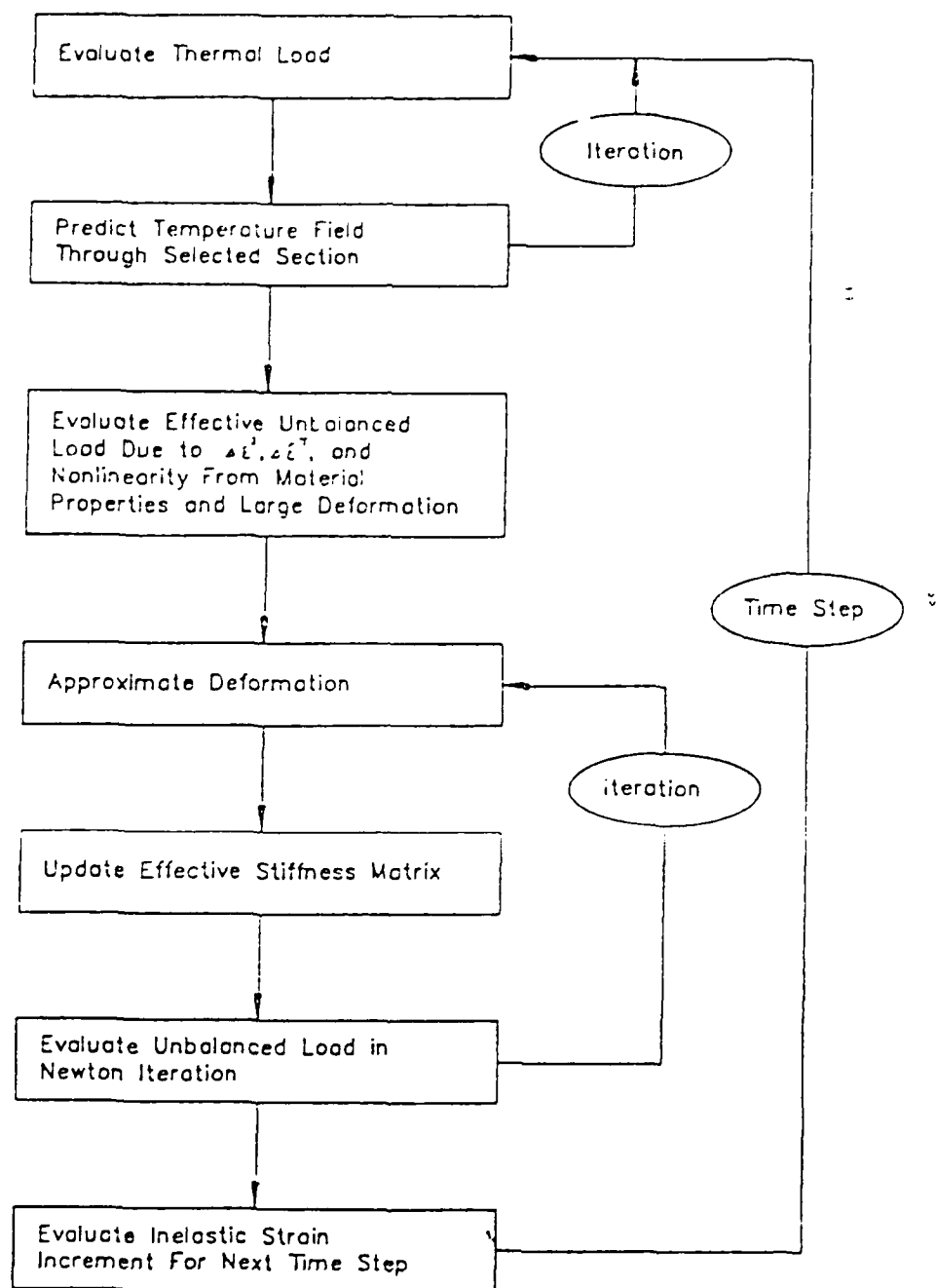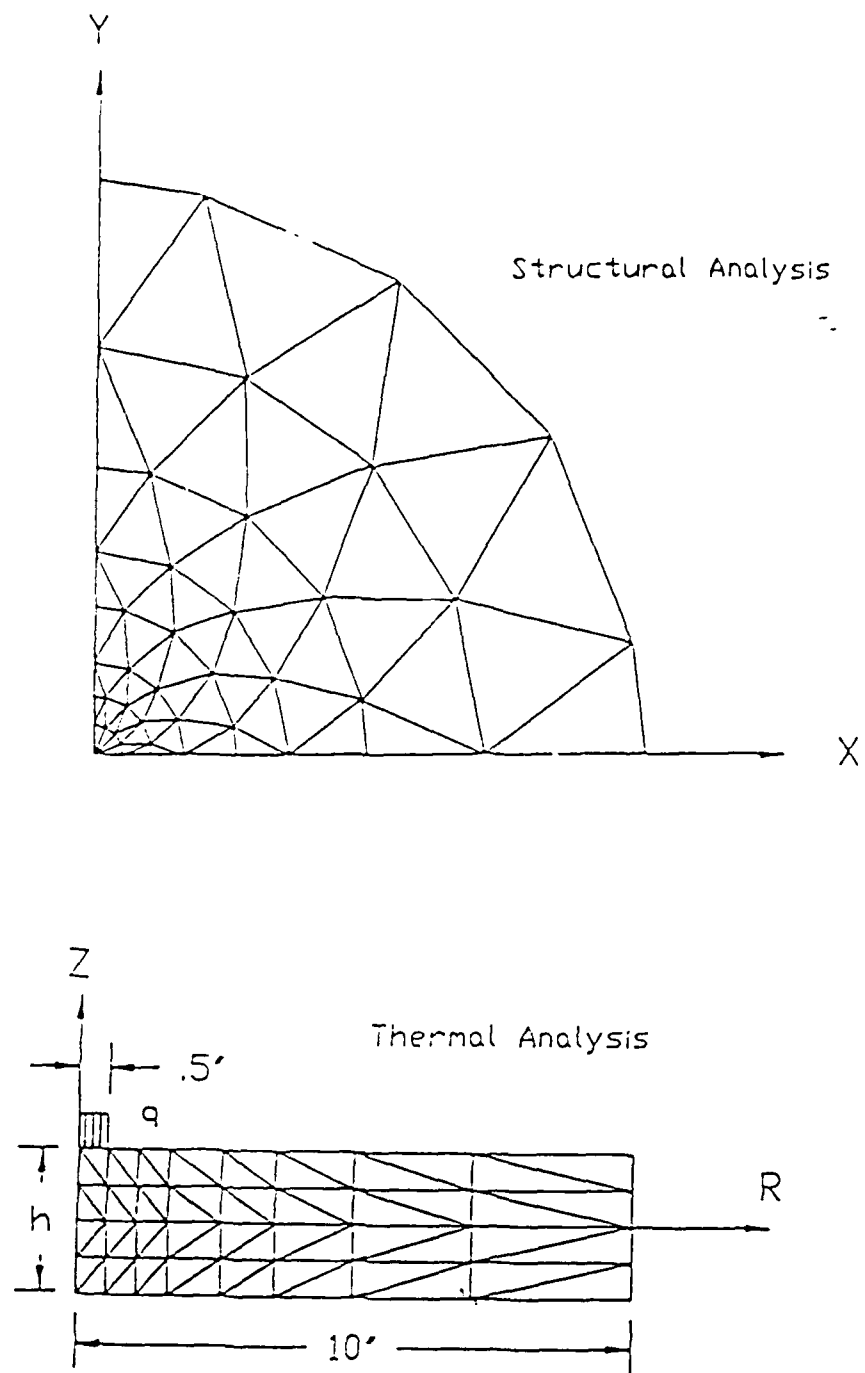
Fig.2 Mesh Diagram of Thermal & Structural Analysis.

21

Fig.3 Center Displacement History

o=60 Btu/in² −sec. h=0.042 in
△ −− w/o geometric effect
o −− with geometric effect
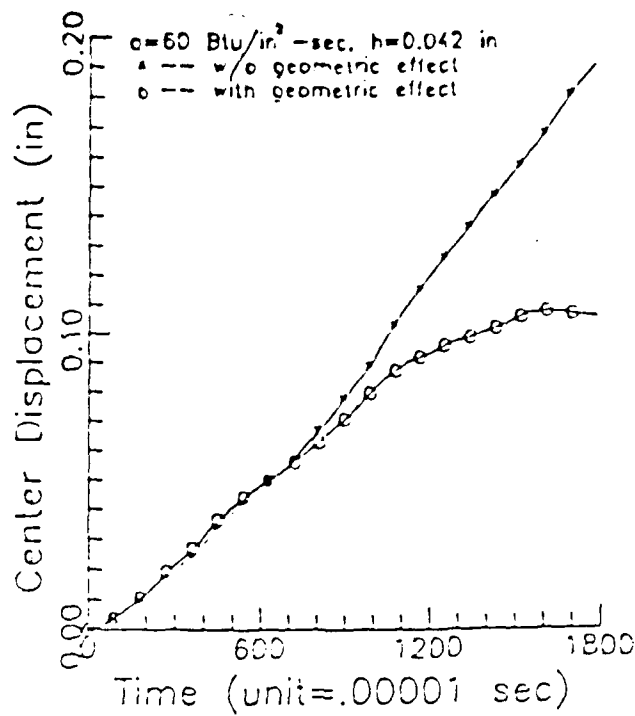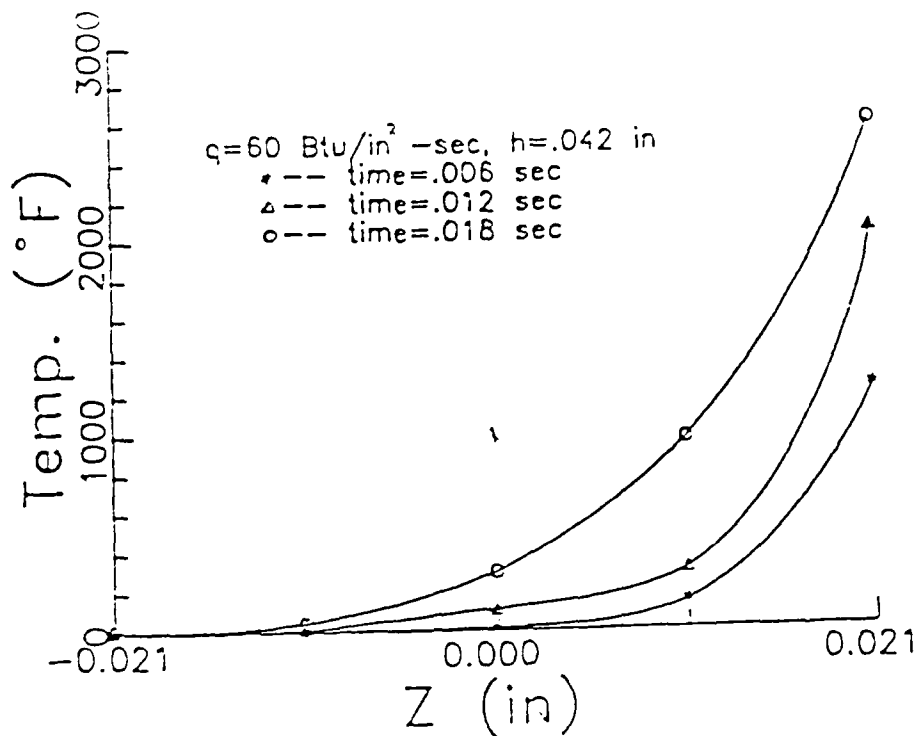
Fig.4 Through Thickness Temperature Distribution

q=60 Btu/in² −sec, h=.042 in
• −− time=.006 sec
△ −− time=.012 sec
o −− time=.018 sec

22
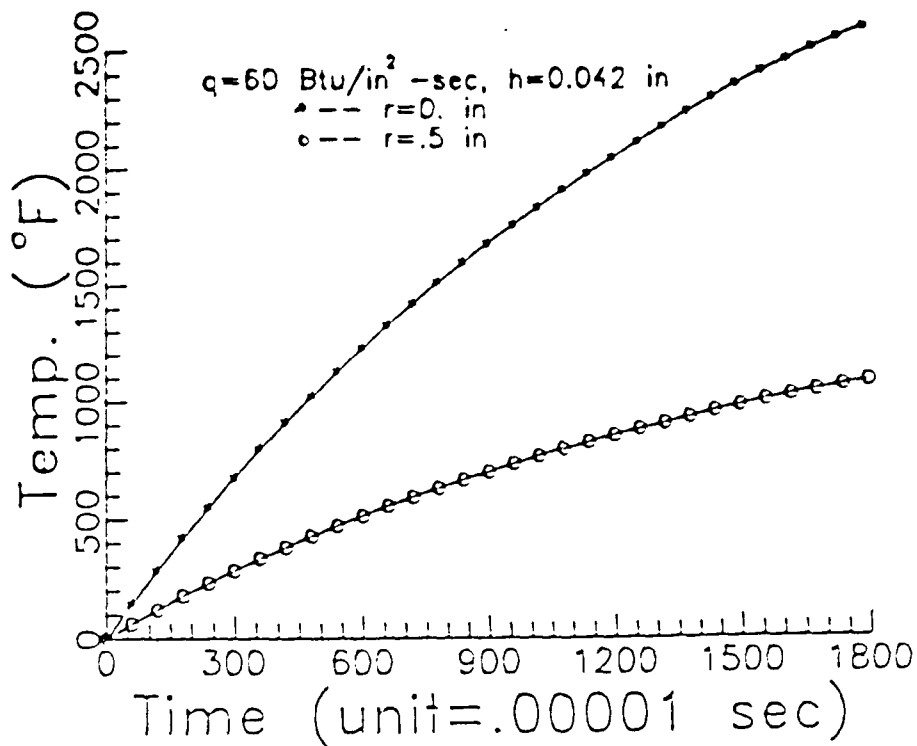
Fig.5 Temperature History at Center of Upper Surface
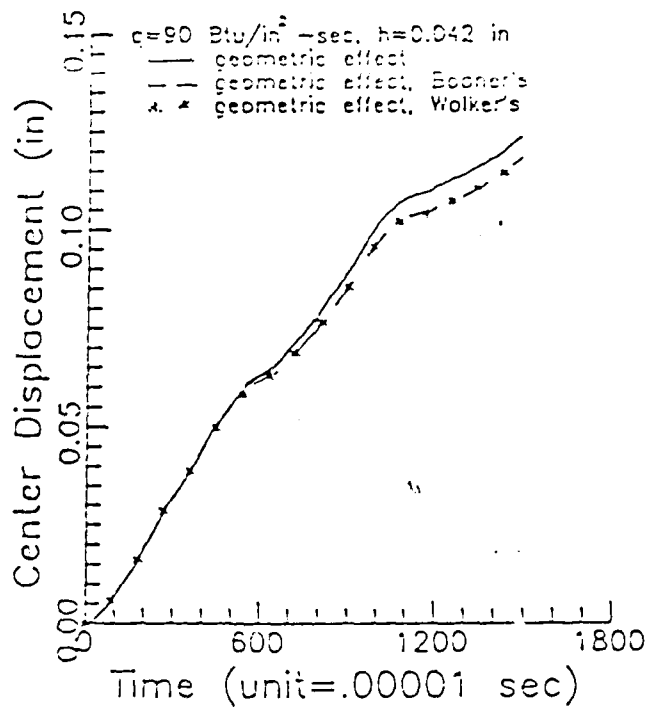
Fig.6 Center Displacement History

23

Time (unit=.00001 sec)
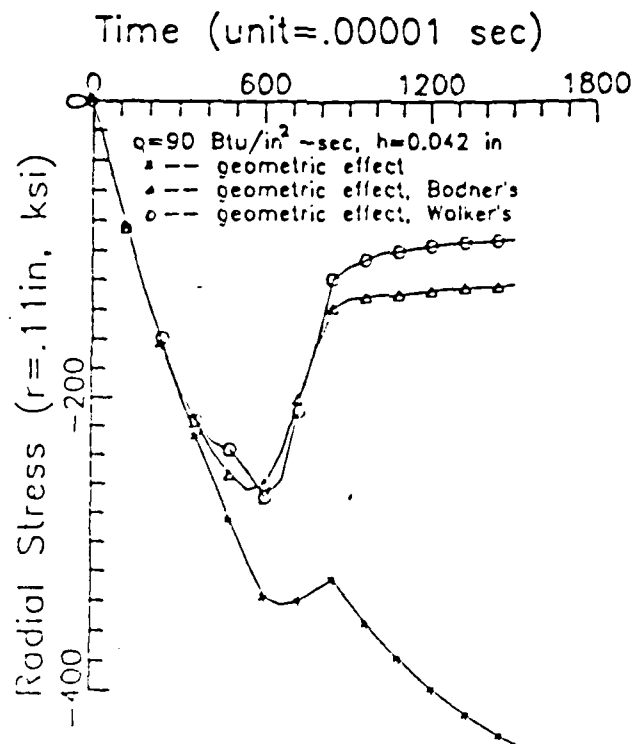
Fig.7 Radial Stress History at r=0.11 in.

Time (unit=.00001 sec)
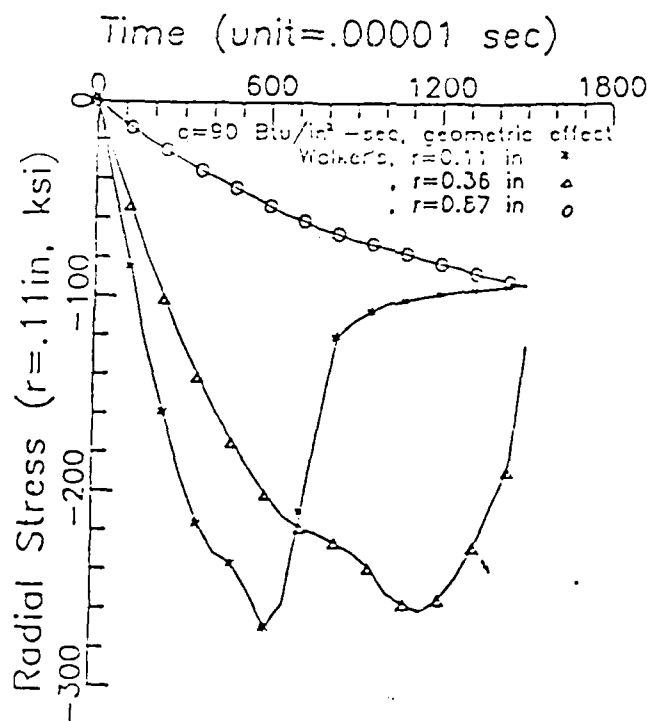
Fig.8 Radial Stress History at Various Positions.
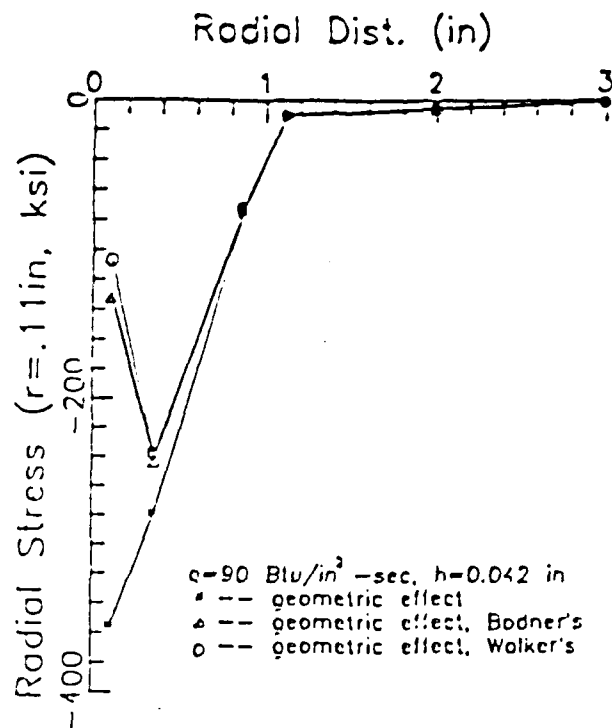
Radial Dist. (in)

Fig.9 Radial Stress Distribution at time=0.01 sec.

Radial Stress (r=.11in, ksi)

$q=90$ Btu/in^2—sec, h=0.042 in
* —— geometric effect
△ —— geometric effect, Bodner's
○ —— geometric effect, Wolker's

Radial Dist. (in)

Fig.10 Hoop Stress Distribution at time=0.01 sec.

Hoop Stress (r=.11in, ksi)

$q=90$ Btu/in^2—sec, h=0.042 in
* —— geometric effect
△ —— geometric effect, Bodner's
○ —— geometric effect, Wolker's

Radial Deformation

0.0008

0.0005

0.0003

0.0000

q=90 Btu/in² −sec, h=0.042 in
▲ −− geometric effect
▲ −− geometric effect, Bodner's
○ −− geometric effect, Wolker's

5

10

Radial Dist. (in)
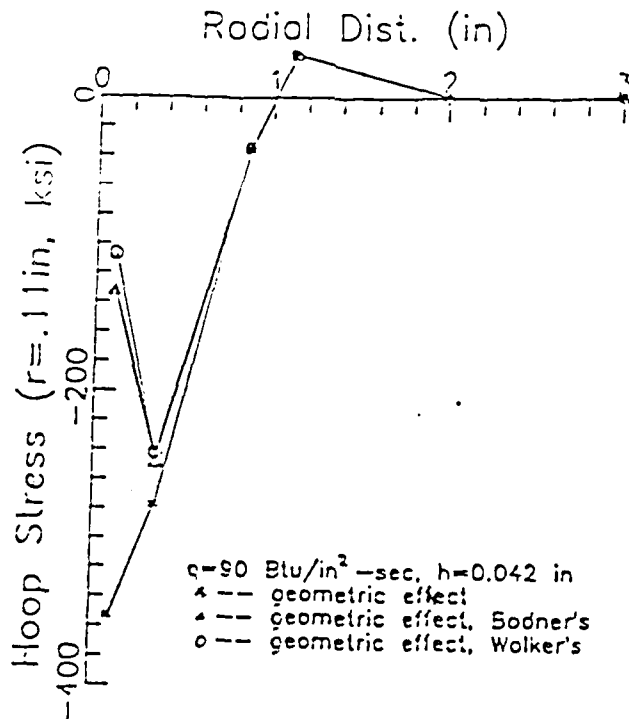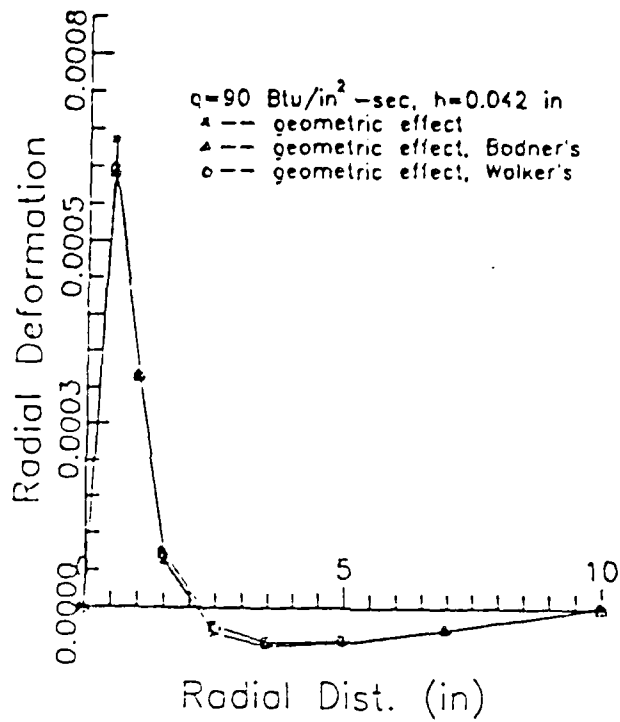
Fig.11 In-plane Deformation at time=0.01 sec.

Radial Dist. (in)

1   2   3

0.000

−0.005

−0.010

−0.015

Radial Inelastic Strain

q=90 Btu/in² −sec, h=0.042 in
* −− geometric effect, Bodner's
○ −− geometric effect, Wolker's
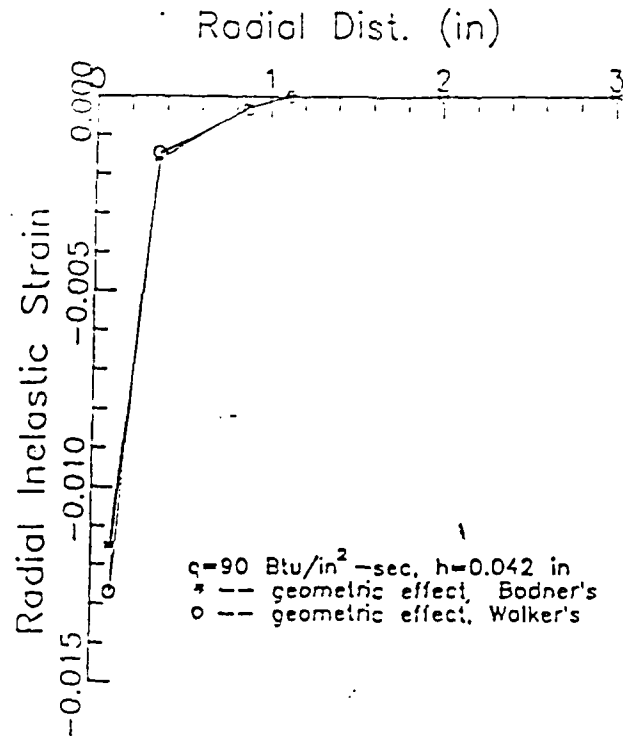
Fig.12 Radial Inelastic Strain Distribution at time=0.01 sec.

26
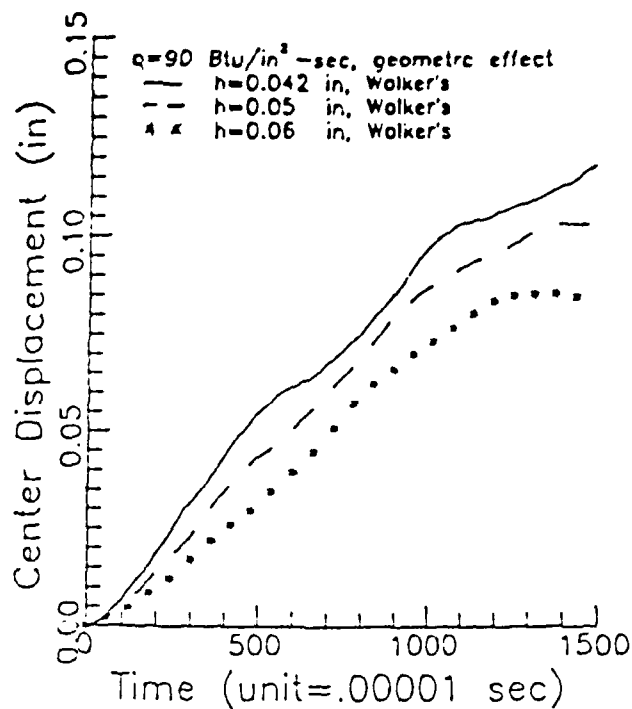
Fig.13 Center Displacement History
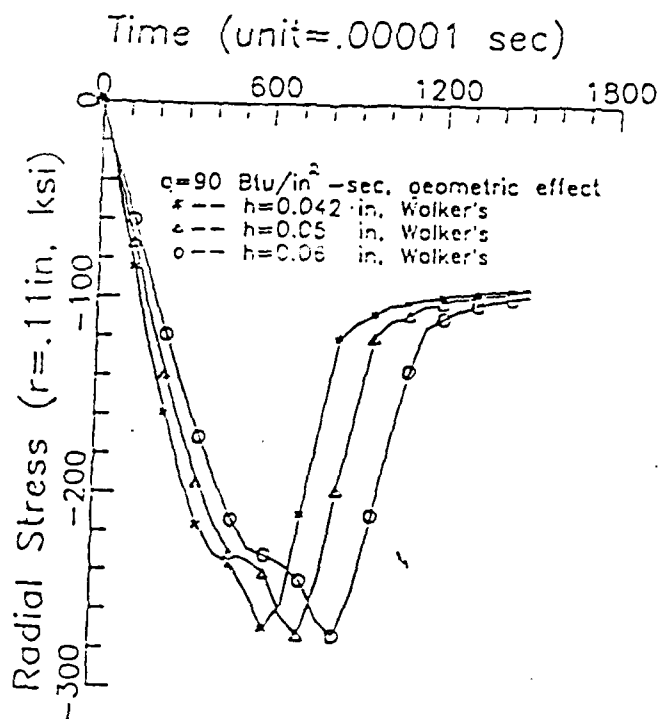
Fig.14 Radial Stress History at r=0.11 in.

27

Radial Dist. (in)

Fig.15 Radial Inelastic Strain Distribution at time=0.01 sec.

c—90 Btu/in² —sec. geometric effect
x —— h=0.042 in. Wolker's
△ —— h=0.05 in. Wolker's
o —— h=0.06 in. Wolker's

q=90 Btu/in² —sec
x —— h=0.042 in
△ —— h=0.05 in
o —— h=0.06 in
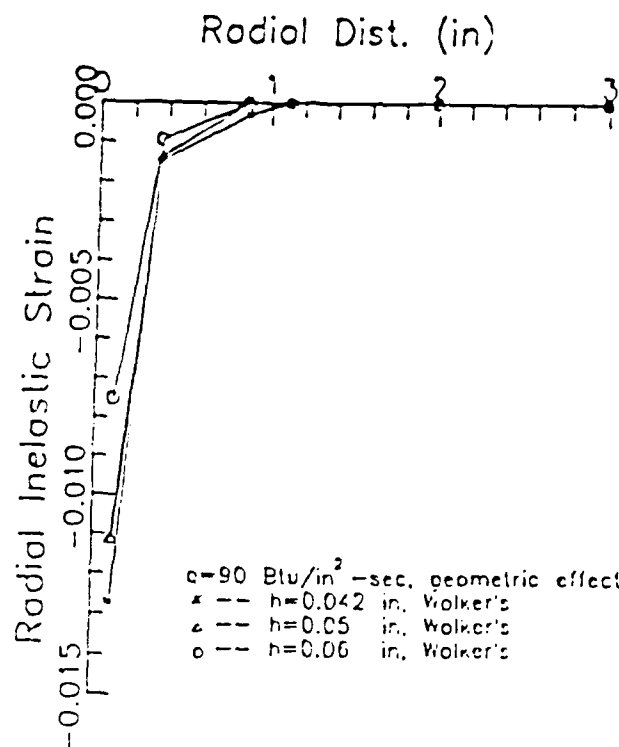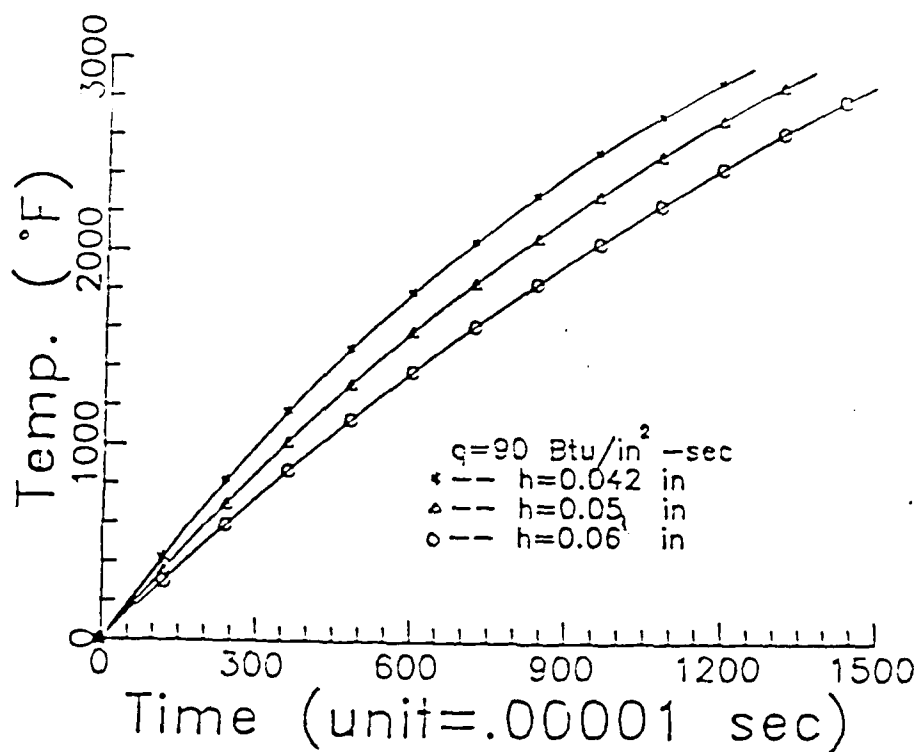
Fig.16 Temperature History at Center of Upper Surface for Various h.

28
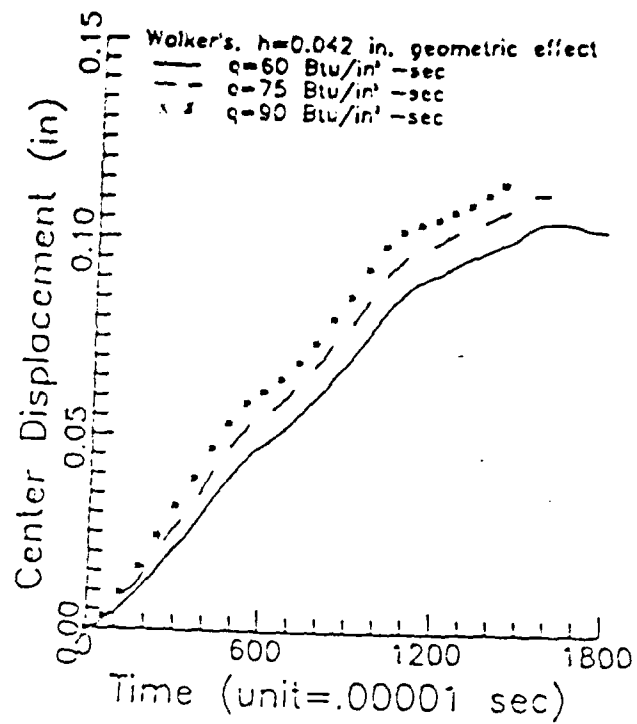
Fig.17 Center Displacement History
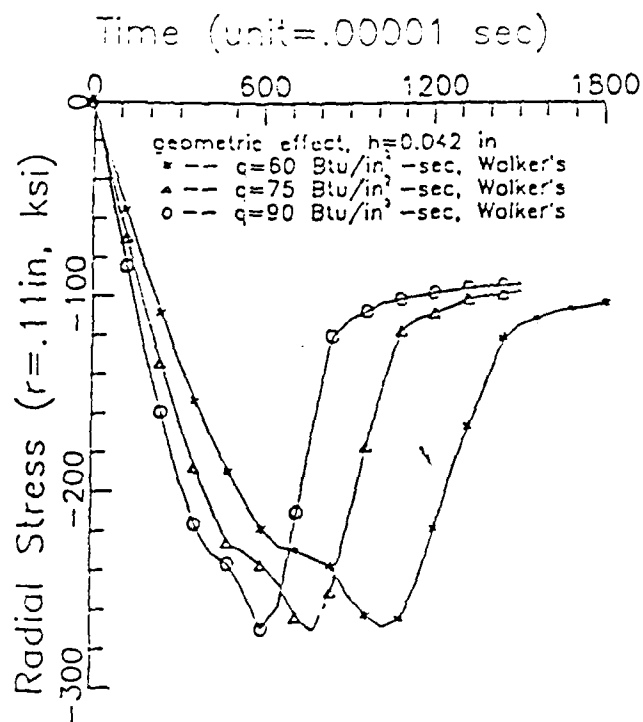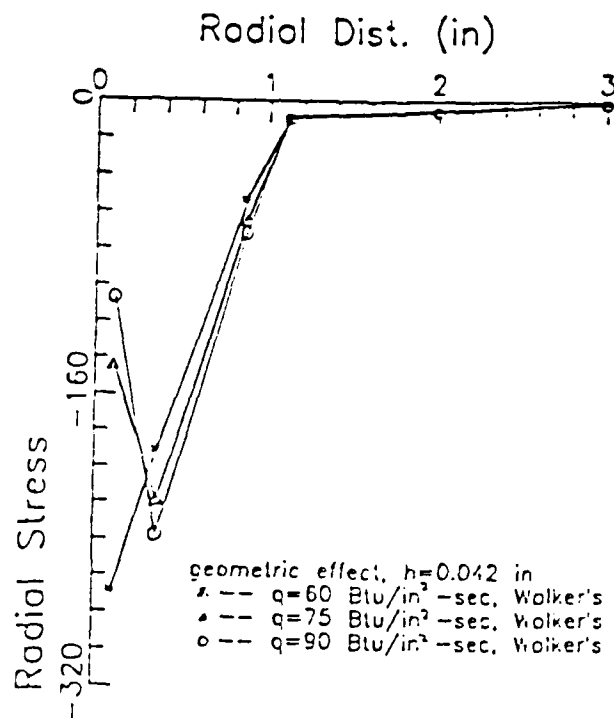

Fig.18 Radial Stress History at r=0.11 in.

29

Radial Dist. (in)

geometric effect, h=0.042 in
*. -- q=60 Btu/in² -sec, Walker's
* -- q=75 Btu/in² -sec, Walker's
o -- q=90 Btu/in² -sec, Walker's

Fig.19 Radial Stress Distribution at time=0.01 sec.

h=0.042 in
* -- q=60 Btu/in² -sec
* -- q=75 Btu/in² -sec
o -- q=90 Btu/in² -sec

Time (unit=.00001 sec)
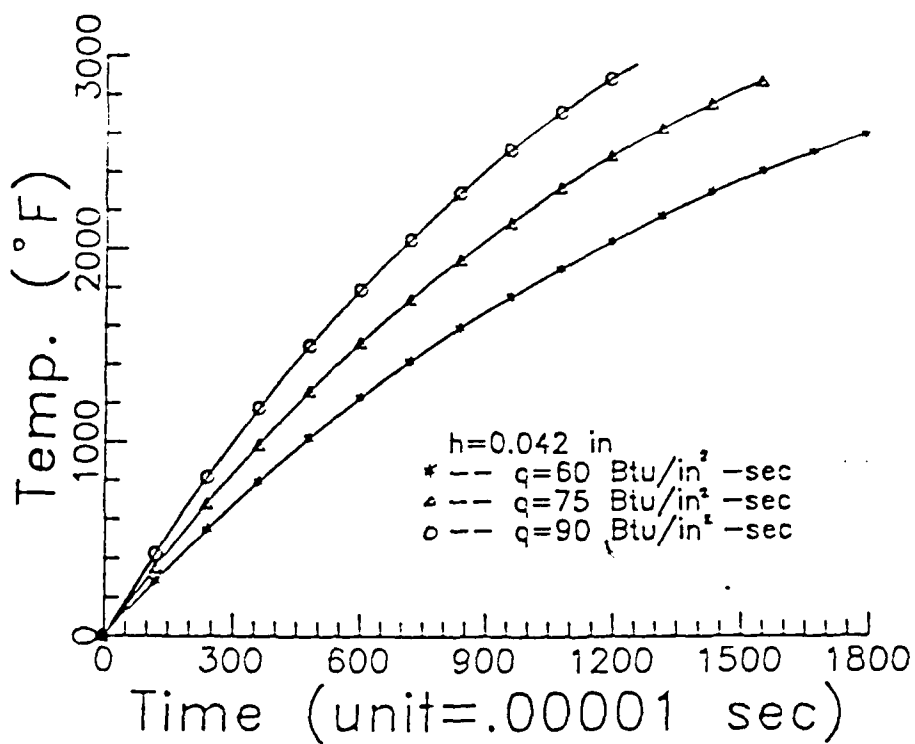
Fig.20 Temperature History at Center of Upper Surface for Various q.

30

APPENDIX 6.2

LASER/STRUCTURE INTERACTION - A COMPARISON
OF THEORY TO EXPERIMENT

P.K. Imbrie[*]

D.H. Allen[**]

H.T. Chang[***]
Texas A&M University
College Station, Texas 77843

Abstract

A comprehensive experimental program has been developed to study the transient response of a viscoplastic plate subjected to rapid heat input. The experiments consisted of irradiating a clamped plate of Hastelloy X with a high energy 15 KW c.w. CO_2 laser, with displacement and temperature serving as measured data. A theoretical model is also being developed for comparison to the experimental results. The model assumes one-way thermomechanical coupling; that is, it is assumed that the temperature field is independent of deformation but not vice versa. The thermal analysis is nonlinear via radiation boundary conditions and temperature dependent thermal conductivities. The structural analysis includes geometric nonlinearity and material viscoplasticity. The experimental procedure and an abbreviated development of the model are described in this paper.

Nomenclature

A_e — area of two-dimensional finite element

$[E_L]$ — matrix relating linear components of strain and deformation

$[E_{NL}]$ — matrix relating nonlinear components of strain and deformation

C_p — coefficient of specific heat at constant pressure

D_{ij} — elastic modulus matrix

f_i — components of body force per unit mass

k — thermal conductivity

m_{ij} — components of finite element mass matrix

n_r, n_z — components of unit outer normal vector in cylindrical coordinates

N, M — components of plate midsurface forces and moments per unit length

N_i — finite element shape functions

q — heat flux input

r — radial coordinate direction

R_i — finite element external force components

t — time

T — temperature

T_r — reference temperature at which radiation is zero

u, v, w — components of plate displacement

u_i — components of displacement in Cartesian coordinates

z — axial coordinate direction

$\bar{\alpha}$ — thermal absorptivity

α_1 — drag stress

α_{2ij} — back stress tensor

ξ_x, ξ_y — components of plate rotation

Γ — boundary of a domain

Γ_e — boundary of a finite element

ϵ — thermal emissivity

ϵ_{ij} — strain tensor

κ_{ij} — plate mid-surface rotations

ϵ_{ij}^E — elastic strain tensor

ϵ_{ij}^I — inelastic strain tensor

ϵ_{ij}^T — thermal strain tensor

ϵ_x, ϵ_y — nodal components of plate rotation

λ — normality coefficient for inelastic strain rate

ρ — mass density

σ — Boltzman's constant

σ_{ij} — stress tensor

---

[*] Lecturer, Aerospace Engineering
[**] Professor, Aerospace Engineering
Member AIAA
[***] Research Engineer, Aerostructures, Inc., Arlington, Virginia

1

σ'_{ij} — deviatoric stress tensor

Ω — interior of a domain

Introduction

The transient response of an aerospace structure exposed to rapid heating may be vastly different from that produced under steady state conditions. For applications such as gas-turbine combustors, rocket nozzles, space structures, and the like, large temperature gradients are commonly induced in a very short period of time. However, due to the complex and severe environment, little experimental data are available for use in developing new methods of analysis where material inelasticity occurs in the structure. Therefore, an experimental program was established to investigate the response of a metallic plate undergoing rapid heating with temperature and displacement as the primary variables of interest. The parameters varied in the experiment included: 1) plate thickness; 2) heat flux; and 3) duration of heat flux.

A solution algorithm has been developed by the authors for predicting the transient response of plates when subjected to rapid heat input. While the model itself is not the subject of this paper, it is presented in abbreviated form and is used to compare theory to experiment. The solution algorithm makes use of one-way thermomechanical coupling (it is assumed that the temperature field is independent of deformation), thermoviscoplastic response, and geometric nonlinearities. The finite element method is used in a two step process to compute the plate response. The thermal analysis is performed first, taking into account such things as nonlinear effects due radiation heat exchange and temperature dependent material properties. The results are then used as input to the structural analysis where nonlinear material response, using Bodner's[1] and Walker's[2] constitutive models and large rotational plate theory are used to compute plate deformation as well as stress and strain. Both the experimental and modelling programs are described in the following sections.

Model Development

The model is presented in abbreviated form in this section. Further details can be found in references 3 and 4. As shown in the flowchart in Fig. 1, the solution algorithm is constructed in two stages: the thermal analysis and the structural analysis. On a given time step, the thermal loads are evaluated. Then the temperature field is solved by the finite element method. Using this temperature field, along with the inelastic strain increment evaluated from the previous time step, yields the thermal strain. The thermal strain results in an unbalanced load from which the deformation field is approximated. An iterative procedure is utilized to bring the solution to convergence for a given time step. The solution is described in further detail below.

Thermal Analysis

An axisymmetric finite element model, developed to include nonlinear radiation boundary conditions, is used to construct the temperature field as a function of r and z for each time step. A typical two-dimensional axisymmetric heat transfer mesh is shown in Fig. 2.

The governing heat transfer equations are as follows:

$$\rho C_p r \frac{\partial T}{\partial t} - \frac{\partial}{\partial r}\left(kr \frac{\partial T}{\partial r}\right) - \frac{\partial}{\partial z}\left(kr \frac{\partial T}{\partial z}\right) = 0 \quad \text{in } \Omega \quad (1)$$

$$kr \frac{\partial T}{\partial r} n_r + kr \frac{\partial T}{\partial z} n_z = \bar{q}\bar{\sigma}r + \varepsilon\sigma r(T_r^4 - T^4) \quad \text{on } \Gamma \quad (2)$$

Equations (1) and (2) may be cast into a Galerkin finite element formulation. Since this part of the model exists in the open literature[5], it is not covered in detail here.

The resulting element equations are of the form

$$C_{ij}\dot{T}_j + k_{ij}T_j = q_i \quad (3)$$

where

$$C_{ij} = \int_{A_e} \rho C_p N_i N_j r dA_e \quad (4a)$$

$$k_{ij} = \int_{A_e} \left(\frac{\partial N_i}{\partial r} rk \frac{\partial N_j}{\partial r} + \frac{\partial N_i}{\partial z} rk \frac{\partial N_j}{\partial z}\right) dA_e$$

$$+ \int_{\Gamma_e} N_i (k_\lambda T_k)^2 N_j r dr \quad (4b)$$

$$q_i = \int_{\Gamma_e} N_i \bar{q}\bar{\sigma}r dr + \int_{\Gamma_e} N_i \varepsilon\sigma T_r^4 r dr_e \quad (4c)$$

A linear triangular axisymmetric element is used in the analysis. Equation (3) for each element is assembled to give the following global system of ordinary differential equations:

$$[c]\{\dot{T}\} + [k]\{T\} = \{Q\} \quad (5)$$

The Crank-Nicholson scheme is then applied temporally to obtain the temperature field with time[6].

Structural Analysis

In the structural analysis, Von Karman theory[7] is assumed for the thin plate bending motion[7], and material nonlinearity and viscoplastic constitution are included in the model. The material nonlinearity is introduced via the inelastic strain tensor, ε_{ij}^I, which is described in the next section.

The strain components are defined as

$$\varepsilon_{ij} = \varepsilon_{ij}^0 + z\kappa_{ij} = \frac{1}{2}(u_{i,j} + u_{j,i})$$

$$+ \frac{1}{2}(u_{3,i}u_{3,j}) + z\kappa_{ij} \quad i,j = 1,2 \quad (6)$$

Utilizing the above in a standard laminate scheme will result in

2

$$\begin{bmatrix} N \\ M \end{bmatrix} = \begin{bmatrix} \bar{A} & \bar{B} \\ \bar{B} & \bar{D} \end{bmatrix} \begin{bmatrix} \epsilon^0 - \epsilon^I - \epsilon^T \\ \kappa \end{bmatrix} \tag{7}$$

where

$$(\bar{A}_{ij}, \bar{E}_{ij}, \bar{D}_{ij}) = \int_{-\frac{h}{2}}^{\frac{h}{2}} D_{ij}(1, z, z^2)\, dz \tag{8}$$

Note that the coupling matrix $[\bar{B}]$ does not disappear due to the through thickness variation of elastic modulus. D_{ij}, which is temperature dependent.

The governing equations for the plate motion are thus derived by satisfying the conservation of linear and angular momentum [8]:

$$N_{x,x} + N_{yx,y} - \rho u_{,tt} = 0 \tag{9}$$

$$N_{xy,x} + N_{y,y} - \rho v_{,tt} = 0 \tag{10}$$

$$[\bar{E}_{1j}\kappa_j + \bar{E}_{1j}(\epsilon_j^0 - \epsilon_{1j}^I - \epsilon_j^T)]_{,xx} +$$

$$[\bar{D}_{2j}\kappa_j + \bar{E}_{2j}(\epsilon_j^0 - \epsilon_j^I - \epsilon_j^T)]_{,yy} +$$

$$2[\bar{D}_{3j}\kappa_j + \bar{E}_{3j}(\epsilon_j^0 - \epsilon_j^I - \epsilon_j^T)]_{,xy} +$$

$$p + N_x w_{,xx} + 2N_{xy} w_{,xy} + N_y w_{,yy} - \rho w_{,tt} = 0 \tag{11}$$

Integrating equations (9) through (11) against variations in the components of the displacement field will result in the following variational principle.

$$\int_A \delta u \, (N_{x,x} + N_{y2,y} - \rho u_{,tt}) \, dxdy +$$

$$\int_A \delta v \, (N_{xy,x} + N_{y,y} - \rho v_{,tt}) \, dxdy +$$

$$\int_A \delta w \, \{[\bar{E}_{1j}\kappa_j + \bar{E}_{1j}(\epsilon_j^0 - \epsilon_{1j}^I - \epsilon_j^T)]_{,xx} +$$

$$[\bar{D}_{2j}\kappa_j + \bar{E}_{2j}(\epsilon_j^0 - \epsilon_j^I - \epsilon_j^T)]_{,yy} +$$

$$2[\bar{E}_{2j}\kappa_j + \bar{E}_{3j}(\epsilon_j^0 - \epsilon_j^I - \epsilon_j^T)]_{,xy} + p +$$

$$N_x w_{,xx} + 2N_{xy} w_{,xy} + N_y w_{,yy} - \rho w_{,tt}\} \, dxdy = 0 \tag{12}$$

Incrementing the field variables, neglecting the third and higher order terms of the displacement increment, and applying finite element discretization results in

$$[M]\{\ddot{u}\}^{t+\Delta t} + [K]\{\Delta u\} = \{R\}^{t+\Delta t} - \{F_1\} - \{F_2\} \tag{13}$$

where $[M]$ is the mass matrix and

$$[K] = [K_{NL}] + [K_L] \tag{14}$$

$$[K_L] = \sum_{n=1}^{n_e} \int_{V_e} [B_{NL}]^{TR} [D]^{t+\Delta t} [B_L] \, dV_e \tag{15}$$

$$[K_{NL}] = \sum_{n=1}^{n_e} \int_{V_e} [B_{NL}]^{TR} [S]^{t+\Delta t} [B_{NL}] \, dV_e \tag{16}$$

Also, $\{R\}$ is the external load vector and

$$\{F_1\} = \sum_{n=1}^{n_e} \int_{V_e} [B_L]^{TR} (\{\sigma\} - [D]^{t+\Delta t}(\Delta\epsilon^I + \Delta\epsilon^T) +$$

$$[\Delta D] (\epsilon^0 + 2\kappa - \epsilon^I - \epsilon^T)) \, dV_e \tag{17}$$

$$\{F_2\} = \sum_{n=1}^{n_e} \int_{V_e} [B_{NL}]^{TR} (-[D]^{t+\Delta t}(\Delta\epsilon^I + \Delta\epsilon^T) +$$

$$[\Delta D] (\epsilon^0 + 2\kappa - \epsilon^T - \epsilon^I)) \, dV_e \tag{18}$$

Solving equation (13) by the Newmark integration scheme will give the first approximation of $\{\Delta u\}$ at time $t+\Delta t$. The Newton Raphson iteration method will give convergence to the nonlinear solution[3,5].

Thermomechanical Constitutive Models

In order to prescribe the forcing functions $\{F_1\}$ and $\{F_2\}$ defined in equations (17) and (18) it is necessary to determine the inelastic strain increment, $\Delta\epsilon_{ij}^I$. This is accomplished by integration of the selected viscoplastic constitutive model. The authors are currently using Walker's model[12], as well as the anisotropic hardening form of Bodner's model[14]. These models are compared critically in reference 11.

Bodner's model assumes

$$\dot{\epsilon}_{ij}^I = \lambda \sigma_{ij}' \tag{19}$$

whereas Walker's model proposes

$$\dot{\epsilon}_{ij}^I = \lambda(\sigma_{ij}' - \omega_{2ij}) \tag{20}$$

where

$$\lambda = \lambda \, (\sigma_{ij}', \sigma_2, \omega_{2ij}) \tag{21}$$

and the above is supplemented by an additional set of evolution laws of the form

$$\dot{\sigma}_{ij}^n = \Sigma_{ij} \, (\epsilon_{k\ell}, \sigma_{k\ell}^v) \tag{22}$$

Equations (19) and (22) are typically numerically stiff, so that numerical integration to obtain ϵ_{ij}^I is not straightforward[13]. Bodner's model is currently being integrated using Euler's forward method, whereas Walker's model is integrated using Euler's backward method[13]. Both models are subincremented on each time step in order to produce accurate values for $\Delta\epsilon_{ij}^I$ on each time increment.

Experimental Program

In order to verify analytical models currently being constructed, an experimental program has been developed to investigate the transient response of a viscoplastic plate subjected to rapid heat input. Of particular interest is the measurement of displacement and

temperature fields for a rectangular plate specimen undergoing rapid heating. The experimental program is divided into two phases: 1) a low energy (<100W/in²) input phase being conducted at Texas A&M University; and 2) a high energy (>1KW/in²) input phase being performed at the Air Force Wright Aeronautics Laboratories using the LHMEL I (Laser-Hardened Materials Evaluation Laboratory) facility.

Low Energy Testing

The low energy, semi-rapid heating experiments make use of a bank of quartz lamps, to irradiate the plate specimens. The purpose of these experiments is two fold: first, they serve as a simulation of the high energy experiments; and second, they produce temperature and displacement fields which change at a much slower rate. Therefore, valuable information with regard to expected experimental results can be gained, in addition to verifying model predictions under less severe conditions.

The heat source for these experiments are tubular quartz lamps with tungsten emitters. A circular heat target zone is obtained by shielding excess energy from the specimen via a water cooled orifice plate, which is fitted with a variable size aperture. This apparatus is attached directly to the specimen support fixture as shown in Fig. 3. The support fixture imposes clamp-like boundary conditions along each edge of a rectangular specimen (details on the support fixture are discussed later in the paper). Insulation shields enclose both sides of the specimen, in order to reduce the amount of heat transfer due to free convection.

Displacement and temperature data are obtained using a PC based data acquisition system, which also serves as the quartz lamp controller. A single DC-operated LVDT, which can be positioned at various radial locations, is used to measure displacements. A coupling tang enables dual measurement of displacement with the LVDT and a precision dial indicator. Measurement of the in-plane temperature field and transverse temperature gradients are made using K-type 30 gage thermocouples intrinsically mounted to the plate specimen. The specimens for this phase of testing were made of 6061-T6 aluminum. This material was selected because it exhibits inelastic deformation at relatively low temperatures (<500°F).

Testing to date has not yielded a high enough input energy to produce a significant specimen temperature rise. In addition, the current aperture system has failed to generate a well defined target zone. Therefore, the orifice plate is being refitted with a lens system that will serve to both condense available heat energy and focus it on the target spot.

High Energy Testing

The high energy, rapid heating experiments made use of an electric discharge 15 KW continuous-wave carbon dioxide laser operating at a wave length of 10.6 µm with a flat-top beam profile, to irradiate the plate specimens. The test apparatus was placed in a nitrogen flood box during irradiation in order to prevent oxidation

of the specimen surface while it was being heated. In addition, instrumentation for measuring temperature and displacement fields, as well as high speed photographic documentation were used and will be discussed in detail below.

A specimen support fixture was designed to impose clamp-like boundary conditions along each edge of a rectangular plate specimen. The superstructure of the fixture was fabricated from 6061-T6 aluminum to support the specimen in the vertical position, as shown in Figs. 4a and 4b. An insert made of 304 stainless steel serves both as a support stiffener and water jacket. A total waste water cooling system is used to provide a uniform and constant plate boundary temperature. Thermocouples were attached to each half of the insert at the mid-position, approximately 0.5 in away from the specimen, to record any temperature variations.

The two piece (with the inserts in place) picture frame style fixture securely clamps the specimen in position, using 24 socket head cap screws torqued to 120 in-lbs. An off-set, staggered screw pattern is used to ensure a uniform clamping zone. In addition, the fixture is indexed with hardened dowel pins so that alignment between the fixture and specimen remains consistent from test to test.

The material selected for this research is Hastelloy X. Hastelloy X is a nickel-chromium-iron-molybdenum alloy that possesses a combination of oxidation resistance and high strength at temperatures in excess of 2200°F. It was selected for this test program primarily for its high temperature characteristics, but also because it is widely used in the research community in conjunction with high temperature constitutive modeling and testing.

The Hastelloy X material was obtained in plate form in nominal thicknesses of 1/16 in, 1/8 in, and 1/4 in, and was used to fabricate a total of 18 specimens (6 of each thickness). The material was received in an annealed condition specified by ASTM 5536 and used without further heat treatment. No micrographic studies were performed to investigate the variations in grain structure or size that existed between the different plate thicknesses.

All specimens were machined to finished dimensions of 13 x 13 in, corresponding to the outer edge of support fixture. Therefore, taking into account the support fixture clamping zone, the effective plate dimensions were reduced to 10 x 10 in. Each specimen was hand sanded with #320 grit sand paper and glass bead blasted to produce a low luster finish. No other special surface treatment, such as anodizing, blueing, or the like, was performed to enhance the thermophysical properties of the material.

An integrated instrumentation package was used to simultaneously measure the displacement and temperature fields of a plate specimen undergoing laser irradiation. The primary instrumentation included: 1) LVDT's (Linear Variable Differential Transformers) for measuring displacement; 2) thermocouples for measuring temperature; 3) a radiant pyrometer for measuring surface brightness temperature; and 4) strain

gages for measuring the plate vibration frequency). A 12 bit, high speed data system (called the PDM) was used to convert the analog output of these transducers and thermocouples to an equivalent binary form at an approximate rate of 1.2 KHz. Once converted, the data were stored on magnetic tape for subsequent conversion to engineering units and any other post-processing. Described below is a more detailed discussion on the implementation of the various pieces of instrumentation.

A total of 11 DC-operated LVDT's were used to sense the out-of-plane displacements resulting from the laser deposition. The outputs of the LVDT's were scaled via the data system, to detect displacements as small as 0.0001 in. at a published maximum frequency response of 15 Hz. The LVDT's were arranged in a symmetric pattern around the heat zone and were rigidly mounted to a support system which was positioned directly behind the specimen, as shown in fig.'s 5a and 5b. In addition, 2 LVDT's were used to monitor relative movement between the LVDT support system and plate fixture.

Measurement of the in-plane temperature field, through-thickness temperature gradients, and non-contact plate surface temperatures, were made using 21 k-type 3D gage thermocouples. The thermocouples were concentrated in a 1 in diameter circle around the heat zone and were arranged in a symmetric pattern for measuring the in-plane temperature field. The through-thickness temperature gradients were measured using thermocouples positioned at the same coordinate locations, but mounted on the front and back of the specimen. All thermocouples were intrinsically mounted to the specimen via a welding operation with the exception of 4 thermocouples. These thermocouples were bead welded junctions which were mounted approximately 0.050 in from the surface of the plate. All thermocouples mounted on the front surface of the plate (the heat side) were Inconel 600 sheated to withstand the extreme temperatures, whereas the thermocouples mounted on the back side of the specimen were insulated using high temperature glass braid. The thermocouples were connected to the data system via a 150°F reference oven, which for this test was left open to room temperature. For thermocouple input, the data system was scaled to record voltage changes on the order of 0.03 mV, which corresponds to a measured temperature resolution of approximately 1.4°F. Thus, taking into account the NBS wire error specification and the above resolution, a maximum temperature uncertainty between 5.38°F and 18.5°F can be expected.

A germanium radiation pyrometer was used to obtain relative measurements of the plate surface brightness temperature. The pyrometer is a high speed transducer, having a peak spectral response at a wavelength of 1.5um and an effective temperature range between 900°F and 5400°F within a target area of approximately 0.0491 in². The pyrometer was aligned to record temperatures within the laser irradiated spot diameter in conjunction with a thermocouple. The output of the pyrometer was fed into the data system for use later in developing an appropriate transfer function for the slower responding thermocouples.

A 350 Ω strain gage was used to measure the dynamic response of the specimen resulting from the rapid heating. The strain gage was mounted parallel with the edge of the plate specimen approximately 2.5 in off center. Since vibration frequencies and not strain magnitudes were of interest, the output of the strain gage was displayed on a visicorder strip chart recorder.

A total of 4 laser/structure interaction experiments have been conducted thus far, representing approximately one third of those planned under this phase of testing. All 4 tests utilized the same 1/16 in thick plate specimen with heat flux and exposure time serving as input test variables (as shown in Table 1) and displacement and temperature fields serving as measured or output quantities. Before testing, the laser beam was characterized in terms of the amount of energy being delivered on target, in addition to the beam width and density. Target energy was measured by reflecting approximately 75 of the total available energy into a torpedo calorimeter. The beam profile was determined by ablation of plexiglass samples as shown in fig. 6, by measuring the plexiglass burn patterns, both the laser target area and beam uniformity in the radial direction can be found. For this experiment, the laser contact spot was found to be ellipsoidal, having major and minor axis length equal to 0.5235 in and 0.5276 in, respectively (this is a result of the beam striking the specimen at a 30° incidence angle in order to prevent energy feedback through the laser pattern).

Figures 7 through 10 show typical output of the thermocouples and LVDT's at discrete locations during laser irradiation (with and without time averaging). In particular, Figs. 7 and 9 show raw data (in engineering units) where there is an apparent electrical noise problem. A power spectrum density analysis indicates that 60 Hz and its harmonics, were present in the data. This resulted in peak-to-peak variations of approximately 44°F and 0.0074 in for temperature and displacement, respectively. Future tests will incorporate real time analog filtering and/or post test digital filtering, in order to resolve this problem. Figures 8 and 10 present the same data as discussed above, except that time averaging has been used.

No comment is made about the validity of the data, except to note the following. First, the typical temperature profile shown in Figs. 7 and 8, indicates the thermocouple did not respond during the laser shot. This should not be interpreted as thermocouple lag. For intrinsically mounted thermocouples, one would expect a response time in the msec time frame. It is presumed that the laser firing sequence caused a voltage shift and saturated the A to D system low. Second, a target zone temperature of 800-1000°F was generally encountered, which was far below the 1500-2000°F temperature expected. Lastly, Figs. 9 and 10 show a typical LVDT data that indicates a drastic displacement reversal during irradiation. That is, the specimen initially deforms in the positive direction (towards the heat source) and then reverse itself, going through a neutral point to assume a negative displacement. The authors are awaiting photographic confirmation, via high speed

5

cameras, to see if this phenomena actually exists.

The primary objective of this first phase of testing was to establish a baseline experimental procedure which would verify analytical models currently under construction. To this end, that objective has been met, with the exception of the following problem areas (which are currently being corrected): 1) energizing and/or firing the laser adversely affected the measured data, both with noise and voltage shifts; 2) there was no explicit indication of when the laser power was on and off the target area; 3) the nitrogen flood box did not provide an inert environment and made photographic documentation difficult; 4) the thermocouple reference junction needed to be below room temperature; 5) a constant aperture setting on the video and high speed cameras made photographic interpretation difficult as the specimen heated up; 6) the pyrometer data was inappropriately scaled; and 7) there was apparent movement of the LVDT support stand during laser deposition.

Comparison of Model to Experiment

Limited results have been obtained with the model for comparison to the experimental results given in the previous section. Experimental constants for Bodner's model have been obtained for hastelloy X, as shown in Table 2. The model has been used to predict the response of the square plate of 1/16 in thickness with spatially and temporally constant heat input of 12.2 Btu/in² sec over a 0.25 in radius spot at the center of the plate. Predicted temperature at the front center of the plate versus time is shown for the first 0.08 sec in Fig. 11, where it can be seen that the plate is heated rapidly to a temperature of about 1300°F. This heating is sufficient to cause a center displacement of approximately 0.03 in (about 33% of the plate thickness), as shown in Fig. 12. The displacement field in turn produces radial and hoop stresses near the plate center which rapidly exceed the material yield point on the front surface, as shown in Figs. 13 and 14. These stresses are induced, in large measure, by the plate bending which occurs near the center of the plate, as shown in Fig. 15.

A comparison between Figs. 8 and 11 shows that the predicted and experimentally observed temperatures are not in agreement. Furthermore, Figs. 10 and 12 demonstrate that the displacement predictions are also not in accord with experimental observations. The authors hasten to point out that both the experimental and theoretical results are first passes, and, as such, no attempt has been made to "massage" either result to match the other. Given the complex nature of both the model and experiment, the discordant results are to be expected. Since there are numerous sources for the disagreement, our current emphasis is on uncovering the most important sources in such a way as to enhance the efficiency of the model.

Briefly, we suspect the following sources of disagreement between the model and experiment:

1) We have reason to suspect that both the LVDT's and thermocouples are giving spurious results for short time spans. We are currently studying this problem.

2) The model assumes that the input source commences instantaneously, whereas the laser output indicates an approximately linear rise time of .003 sec. We are modifying the model to account for this.

3) Initial indications are that the input heat source is not spatially homogeneous, thus producing a temperature field which is not axi-symmetric.

4) Currently, we can measure only the amount of heat energy being delivered on target, future tests will try to measure the amount of energy being reflected by the specimen.

5) The very rapid heat input may cause thermal waves which are not predicted by our parabolic heat equation. We are thus considering various hyperbolic forms of the heat equation.

6) The computer code currently requires one CPU day on a VAX 8880 (3 real time days) to produce the first 0.08 sec of predicted response. We are attempting to improve the computational efficiency of the model so that longer term predictions can be obtained.

Conclusion

It is obvious that the experimental results are not in agreement with the model at this point in time. While the authors cannot say with certainty what the cause for discrepancy are, it is the general feeling here that the experimental program needs to be refined considerably before a critical comparison of the model and experiments will yield fruitful results. We are currently making progress in both directions.

Acknowledgement

References

1. Bodner, S.R. and Partom, Y., "Constitutive Equations for Elastic-Viscoplastic Strain-hardening Materials," Journal of Applied Mechanics, Vol. 42, No. 2, pp. 385-389, 1975.

2. Walker, K.P., "Representation of Hastelloy-X Behavior at Elevated Temperature with a Functional Theory of Viscoplasticity," ASME J. Enc. Mat. & Tech., 1982.

3. Chang, H.T. and Allen, D.H., "A Finite Element Analysis of a Viscoplastic Plate Subjected to Rapid Heating," to appear in Mechanics of Structures and Machines an International Journal, 1988.

4. Chang, H.T. and Allen, D.H., "Analysis of Viscoplastic Plates Subjected to Rapid External Heating," Proceedings 29th AIAA/ASME/ASCE/AHS Structures, Structural Dynamics and Materials Conference, Part III, pp. 1640-1647, 1988.

5. Lutz, J.D., Allen, D.H., and Haisler, W.E. "A Finite Element Model for the Thermoelastic Analysis of Large Composite Space Structures," Journal of Spacecraft and Rockets, Vol. 24, No. 5, pp. 430-436, 1987.

6. Moshaiov, A. and Vorus, W.S., "Elastic-Plastic Plate Bending Analysis by a Boundary Element Method with Initial Plastic Moments," Int. J. Solids Structures, Vol. 22, pp. 1213-1229, 1986.

7. Timoshenko, S.P. and S. Woinowsky-Krieger, Theory of Plates and Shells, McGraw-Hill, New York, 1959.

8. Ashton, J.E. and Whitney, J.M., Theory of Laminated Plates, Technomic, Connecticut, 1970.

9. Bathe, K.J., Finite Element Procedures in Engineering Analysis, Prentice-Hall, Englewood Cliffs, 1982.

10. Chan, K.S., Lindholm, U.S., Booner, S.R., and Walker, K.P., "A Survey of Unified Constitutive Theories," Non-Linear Constitutive Relations for High Temperature App. - 1984, NASA CP 2369, pp. 1-24, 1985.

11. James, G.H., Imbrie, P.K., Hill, P.S., Allen, D.H., and Haisler, W.E., "An Experimental Comparison of Current Viscoplastic Models at Elevated Temperature," J. Engr. Mat. Tech., Vol. 109, pp. 130-139, 1987.

12. Imbrie, P.K., James, G.H., Hill, P.S., Allen, D.H., and Haisler, W.E., "An Automated Procedure for Material Parameter Evolution and Uncertainty Analysis for Viscoplastic Constitutive Models," to appear in J. Engr. Mat. Tech., 1988.

13. Haisler, W.E. and Imbrie, P.K., "Numerical Considerations in the Development and Implementation of Constitutive Models," NASA CP 2369, NASA Lewis Research Center, pp. 169-186, 1985.

14. Tong, M., NASA Lewis Research Center, personal correspondence.

Table 1. Laser Parameters for the Specified Tests

Test	Shot Number	Incident Energy (KW)	Beam Area (cm^2)	Heat Flux (KW/cm^2)	Shot Duration (sec)
1	49540	1.4	1.4	1	5.0
2	49541	2.8	1.4	2	3.0
3	49546	4.2	1.4	3	2.0
4	49550	7.0	1.4	5	1.2-1.6

Table 2. Booner-Partom Model Material Constants for Hestelloy X

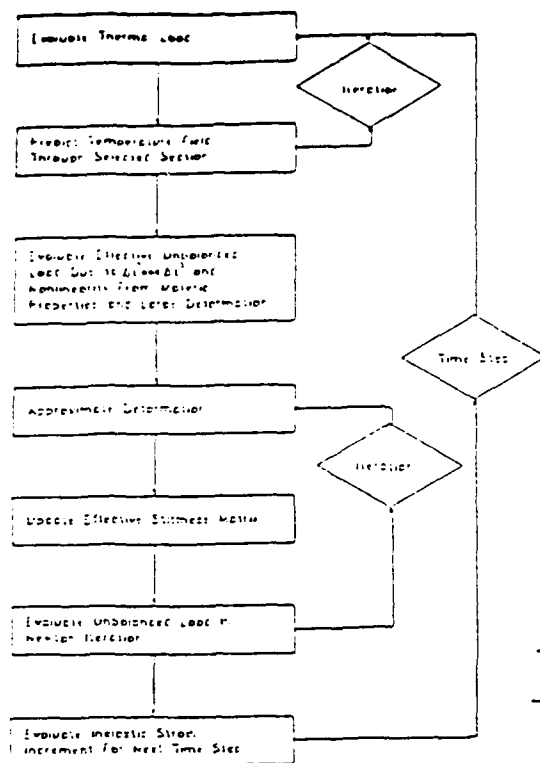| Constant		Temperature		
		Room Temp	1200°F	1600°F
n	1.0	1.0	1.0	0.75
D_0	$10E4$	$10E4$	$10E4$	$10E4$
$m_1 - MPa^{-1} (KSI^{-1})$		0.02 (1.38E-4)	0.1 (6.89E-4)	0.1 (6.89E-4)
$\bar{m}_2 - MPa^{-1} (KSI^{-1})$		1.8 (1.24E-2)	2.4 (1.65E-2)	2.4 (1.65E-2)
$m_3 - MPa^{-1} (KSI^{-1})$		0.001 (6.89E-6)	0.01 (6.89E-5)	.01 (6.89E-5)
$z_0 - MPa (KSI)$		1200 (1.74E5)	1550 (2.248E5)	600 (8.7E4)
$z_1 - MPa (KSI)$		2000 (2.9E5)	2000 (2.9E5)	2000 (2.9E5)
$z_2 - MPa (KSI)$		1200 (1.74E5)	1550 (2.248E5)	600 (8.7E4)
$z_3 - MPa (KSI)$		1200 (1.74E5)	800 (1.16E5)	500 (7.25E4)
$A_1 - sec^{-1}$		0	6.5E-7	6.5E-7
$A_2 - sec^{-1}$		0	6.5E-7	6.5E-7
r_1	0.98	0.98	0.98	0.98
r_2	0.98	0.98	0.98	0.98
$E - MPa (KSI)$		2.07E6 (3.002E7)	1.61E6 (2.335E7)	1.37E6 (1.987E7)

Fig. 1 Flowchart of Solution Algorithm
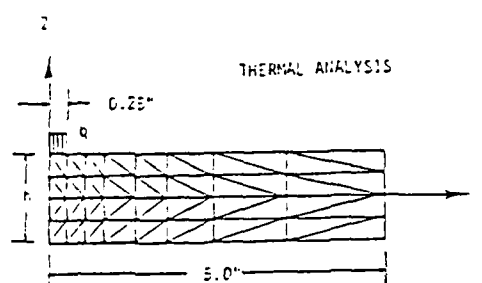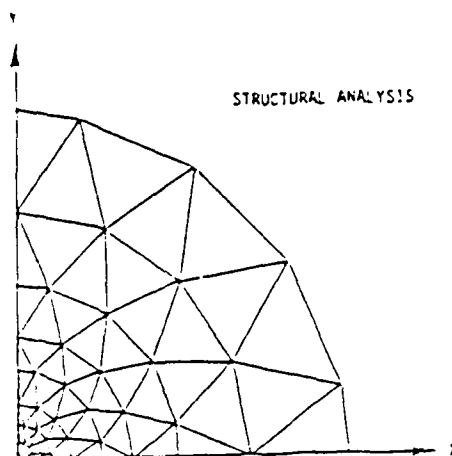

STRUCTURAL ANALYSIS
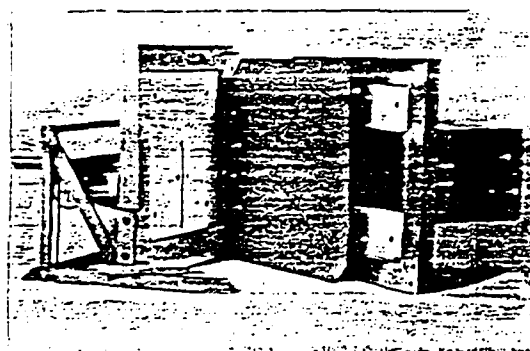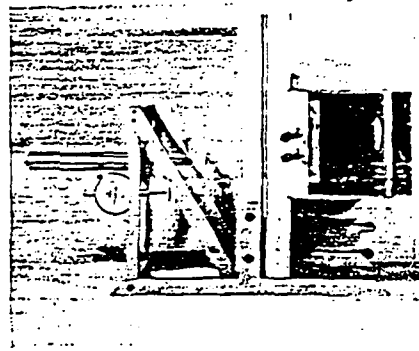
THERMAL ANALYSIS

0.25"

Q

5.0"

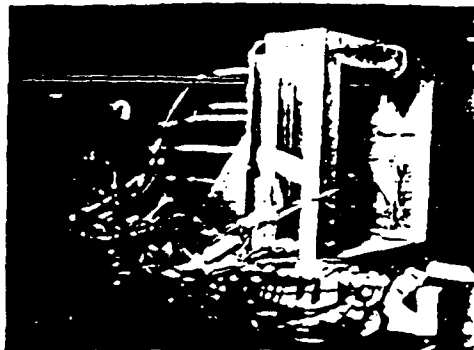Fig. 2 Mesh Diagram of the Thermal and
Structural Analysis

a) Test Frame - Assembly View
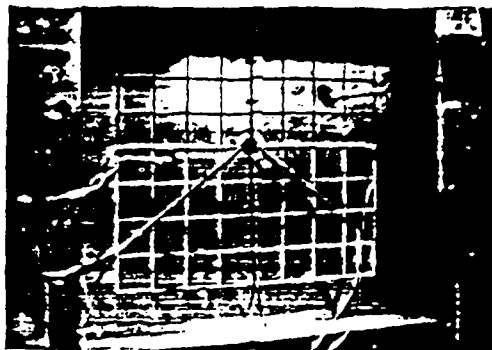
b) Test Frame - Side View

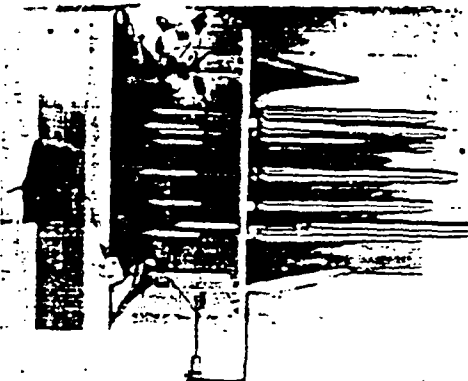Fig. 3 Low Input Heat Energy Test Frame

8

a) Support Structure - Side View   b) Support Structure - Front View

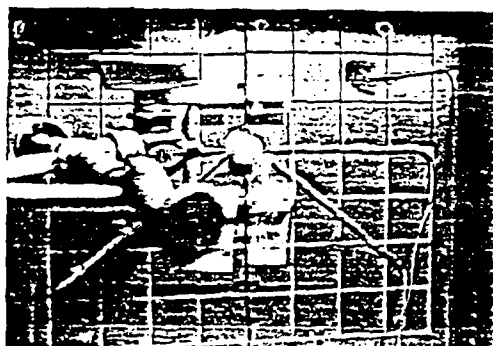Fig. 4 Plate Specimen Support Fixture

a) LVDT Support Stand - Top View   b) LVDT Support Stand - Side View

Fig. 5 LVDT Support Stand Positioned Behind the Specimen

a) Before Ablation   b) After Ablation

Fig. 6 Plexiglass Samples Used to Measure the Laser Beam
Width and Density
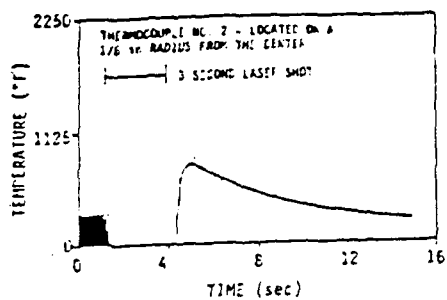
Fig. 7 Typical Thermocouple Output for a 2 KW/cm² 3 Second Duration Test
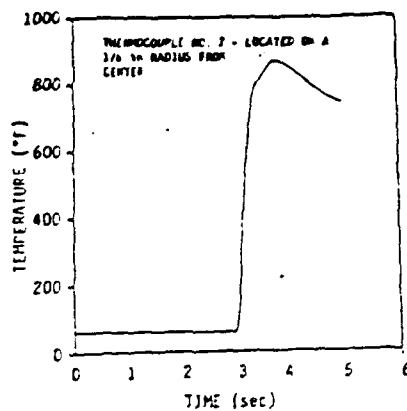
Fig. 8 Time Averaged Thermocouple Output for a 2 KW/cm² 3 Second Duration Test
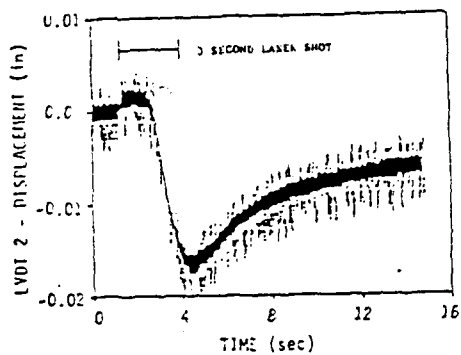
Fig. 9 Typical LVDT Output for a 2 KW/cm² 3 Second Duration Test
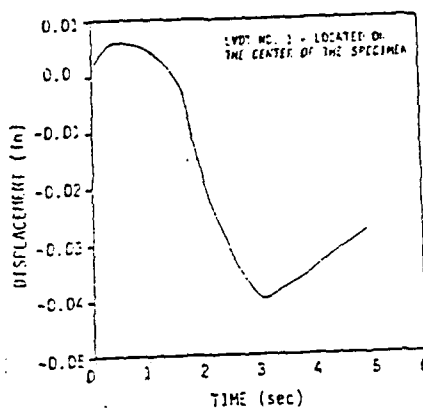
Fig. 10 Time Averaged LVDT Output for a 2 KW/cm² 3 Second Duration Test
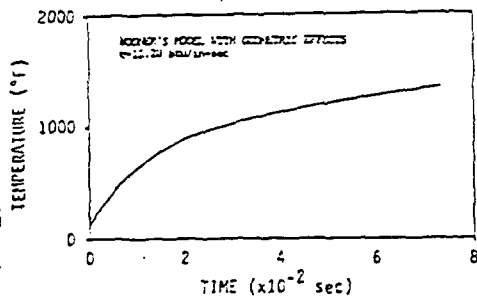
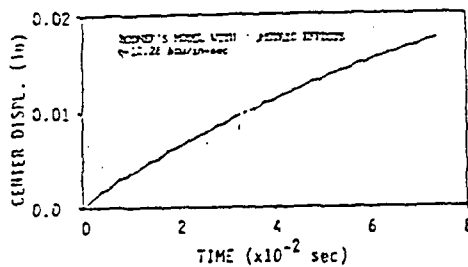Fig. 11 Predicted Temperature at the Front Surface and Center of the Plate

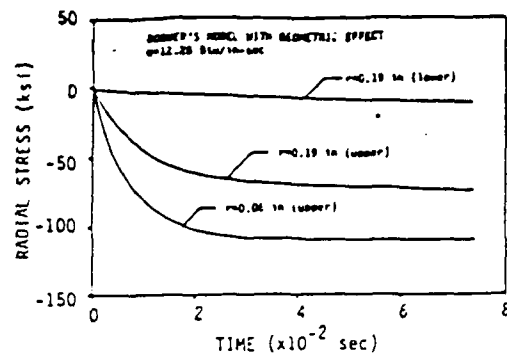Fig. 12 Predicted Displacement at the Center of the Plate

10
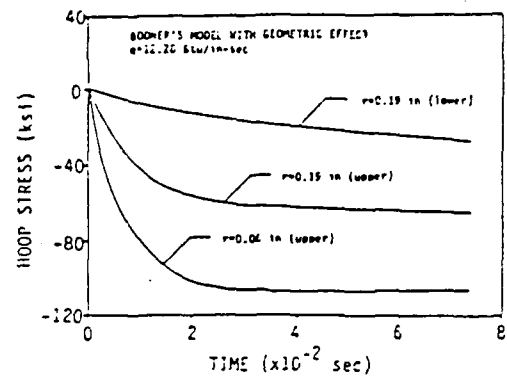
Fig. 13 Radial Stress At Various
Locations

Fig. 14 Hoop Stress at Various
Locations
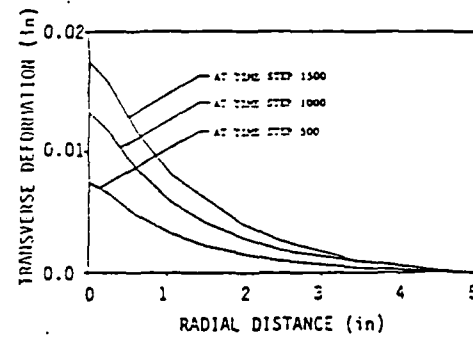

Fig. 15 Transverse Deformation
at Various Times

11

DISCLAIMER NOTICE

**THIS DOCUMENT IS BEST QUALITY
PRACTICABLE. THE COPY FURNISHED
TO DTIC CONTAINED A SIGNIFICANT
NUMBER OF PAGES WHICH DO NOT
REPRODUCE LEGIBLY.**